Assessing the role of cold-shock protein C: A novel regulator of *Acinetobacter baumannii* biofilm formation and virulence

Brooke R. Tomlinson, Grant A. Denham, Robert S. Brzozowski, Jessie L. Allen, Prahathees J. Eswara, & Lindsey N. Shaw*

Department of Cell Biology, Microbiology and Molecular Biology, University of South Florida, 4202 East Fowler Avenue, ISA 2015, Tampa, FL 33620-5150, USA

***Correspondence:** Lindsey N. Shaw (shaw@usf.edu)

Abstract: *Acinetobacter baumannii* is a formidable opportunistic pathogen that is notoriously difficult to eradicate from hospital settings and can spread quickly via healthcare personnel despite preventive measures. This resilience is often attributed to a proclivity for biofilm formation, which grants *A. baumannii* a higher tolerance towards external stress, desiccation, and antimicrobials. Despite this, little is known regarding the mechanisms orchestrating *A. baumannii* biofilm formation. Herein, we performed RNA-seq on biofilm and planktonic populations for the multidrug resistant isolate, AB5075, and identified 438 genes with altered expression. To assess the potential role of genes upregulated within biofilms, we tested the biofilm forming capacity of their respective mutants from an *A. baumannii* transposon library. In so doing, we uncovered 24 genes whose disruption led to reduced biofilm formation. One such element, cold shock protein C (*cspC*), produced a mucoidal, non-mucoviscous colony phenotype. RNA-sequencing of this mutant revealed the down regulation of pili and fimbriae in the *cspC* mutant, which would explain the decreased biofilm observed. Using MIC assays, we note that the mutant displayed increased antibiotic tolerance that we hypothesize is mediated by overexpression of multi-drug efflux pumps and altered mRNA stability of their corresponding transcriptional repressor. Finally, we show that CspC is required for survival during oxidative stress and challenge by the human immune system, and plays a pivotal role during systemic infection. Collectively, our work identifies a cadre of new biofilm associated genes within *A. baumannii* and provides insight into the global regulatory network of this emerging human pathogen.

Introduction

Acinetobacter baumannii is formidable pathogen that causes over 8,000 cases of multidrug resistant infections annually in the United States and is recognized globally as an urgent health threat (1, 2). This bacterium gained a foothold in the US healthcare system in 2003-2005 when injured service members returned home from the Iraq conflicts harboring *A. baumannii* infections (3), earning it the nickname “Iraqibacter.” Since then, a number of outbreaks have occurred in the US, several of which impacted multiple hospitals (4-6). Fundamental to success of this pathogen is the ability to persist on surfaces for prolonged periods (7-10), the rapid spread via healthcare personnel despite conventional prevention measures (11-13), and its genomic plasticity, driving rapid acquisition of antibiotic resistance (14). Thus, it has been suggested that *A. baumannii* employs a ‘persist and resist’ strategy, as opposed to a particular set of toxins or molecular determinants that may otherwise dictate an organism’s potential for virulence (reviewed in (15)).

Like many bacteria, the resilience of *A. baumannii* is often attributed to a proclivity towards biofilm formation and its ability to respond to external stress (16). Biofilms are multicellular aggregates surrounded by exopolymeric substance (EPS), which consists of extracellular DNA, proteins, and polysaccharides (17-19). Biofilms exhibit greater resistance to antimicrobials due to reduced diffusion of antibiotics through the multilayered matrix (20) and physiological heterogeneity of the bacterial community (21), which ultimately promote infection chronicity. These factors also contribute to tolerance of environmental stress, such as desiccation (16), which significantly

enhances *A. baumannii* persistence in hospital settings. Despite this, only a handful of contributing factors and conditions for *A. baumannii* biofilm formation have been identified (reviewed in (22) and (23)). In particular, pili production plays a pivotal role in the first step of biofilm initiation: the irreversible attachment of bacteria to a surface. Two highly conserved, essential *A. baumannii* attachments factors have been identified to date, chaperone-usher pili (Csu) and outer membrane protein A (OmpA) (22, 24, 25). With regards to the latter, OmpA has been shown to facilitate attachment to abiotic surfaces as well as epithelial cells (25). Comparatively, the Csu assembly system (CsuA/B, CsuA-E) seems to have a more critical role mediating attachment to abiotic surfaces and purportedly does so by hydrophobic interaction with structurally variable substrates, including plastic and glass (24, 26). Transcriptional regulation of the *csu* operon is governed by the BfmRS two-component regulatory system (27), although whether this is by direct or indirect means remains unresolved. During sub-MIC antibiotic treatment, BfmRS also enhances the expression of the major capsular biosynthesis gene cluster (K locus) to promote capsule production, another major biofilm determinant (28). Previous work on *Acinetobacter baumannii* and its non-pathogenic relative, *Acinetobacter baylyi,* has shown that capsule production augments desiccation tolerance, which enhances biofilm survival on surfaces for prolonged periods (16, 29, 30). Overall, capsule production is important for *Acinetobacter* desiccation tolerance, biofilm integrity, and persistence, and the regulatory network for capsule production is intertwined with that of pili production and biofilm formation.

To identify novel factors which drive *A. baumannii* biofilm formation, herein we implemented a transcriptomic approach, comparing the global expression profiles of biofilm to that of planktonically growing counterparts. We then identified genes for which transcription was enriched within biofilm, obtained mutants harboring transposons disrupting these genes, and screened for changes in biofilm integrity. In so doing, we identified 24 genes whose disruption resulted in a notable decrease in biofilm mass compared to wildtype. During this screen, we identified one such factor, cold-shock protein C (CspC), disruption of which resulted in a mucoidal, but non-mucoviscous, colony phenotype. Cold-shock proteins (Csps) have a demonstrated importance in cell aggregation (31), extracellular polysaccharide production, and membrane fluidity in other organisms (32). Furthermore, Csps are multifunctional proteins, which can have pleiotropic functions as transcriptional regulators and RNA chaperones (33). Thus, these proteins can have impacts at the transcriptional, post-transcriptional, and translational levels (reviewed in (34, 35)). Although Csps often play important roles in bacterial stress response, they have not been previously implicated in the regulation of *A. baumannii* biofilm formation. In this work, we reveal that disruption of *cspC* leads to enhanced tolerance to polysaccharide degradation, altered antibiotic resistance profiles, and diminished abiotic surface adherence. The *cspC* mutant also exhibited diminished survival in a murine model of infection. Collectively, these findings establish CspC as a novel regulator of *A. baumannii* biofilm formation and disease causation.

Methods

Bacterial strains and growth conditions: Bacterial strains used for this study are listed in Table 1. *A. baumannii* and *Escherichia coli* strains were routinely cultured in lysogeny broth (LB) with shaking or on LB agar at 37°C. When appropriate, media was supplemented with tetracycline and hygromycin at a final concentration of 5 µg/mL and 160 µg/mL respectively. *A. baumannii* biofilm formation was assessed as described previously for microtiter plate biofilms (38) with slight modifications. Briefly, overnight cultures were normalized to an OD_{600} of 5.0 in phosphate-buffered saline (PBS), before 20 µL was added to 180 µL of fresh LB in 96-well microtiter plates for a final OD_{600} of 0.5. For assays incorporating strains harboring pMQ557, LB was supplemented with hygromycin.

Mutant strain confirmation and complement strain construction: Transposon mutant strains were obtained from the *A. baumannii* AB5075 transposon mutant library (37). Transposon insertion was confirmed for the *cspC* transposon mutant by PCR and sequencing using primers OL5087 and OL5088 which flank *cspC* (all primers are listed in Table S1). A *cspC*-complement PCR fragment was amplified using primers OL5088 and OL5214 and cloned into plasmid pMQ557. In addition to the full length of *cspC*, the complement fragment includes 382 nucleotides immediately upstream and 97 nucleotides directly downstream of the *cspC* coding region to ensure the native promoter and full-length mRNA (as revealed by RNA-seq) were incorporated. Complementation plasmid pMQ557::*cspC* was transformed into chemically competent

E. coli (DH5α) and confirmed using pMQ557 screening primers OL4163 and OL4164 followed by sequencing. Plasmid containing the correct sequence was transformed into the *cspC* transposon mutant strain via electroporation (44) to generate the complement strain, *cspC*$^{+}$. Given that vector is present in *cspC*$^{+}$, the empty pMQ557 vector was also transformed into the wildtype parental strain and *cspC* transposon mutant strain (*cspC*$^{-}$). For all assays *cspC*$^{+}$, wildtype and *cspC* mutant strains bearing pMQ557 were used for comparison throughout.

RNA sequencing: *A. baumannii* biofilm formation was initiated in 96-well microtiter plates as described above in biological triplicate for 24 h at 37°C in a static incubator. To collect planktonic samples, 75 μL of supernatant was removed from each well and pooled. Planktonic cells were immediately combined with 5 mL of ice-cold PBS, and pelleted by refrigerated centrifugation. For biofilm samples, the remaining supernatant was removed and biofilm containing wells were washed three times with 200 μL of ice-cold PBS. Ice-cold PBS was added a final time and pipetted vigorously to disrupt biofilm cells. Biofilm cells from different wells were pooled, immediately combined with an additional 5 mL of ice-cold PBS, and pelleted by refrigerated centrifugation.

For collection of AB5075 wildtype and AB5075 *cspC::tn* mutant samples, strains were grown in LB overnight with shaking at 37°C in biological triplicate. Overnight cultures were diluted 1:100 into 5 mL of fresh LB, grown to exponential phase, and subsequently used to seed new 100 mL cultures at OD_{600} 0.05. Samples were harvested after 3 hours

of growth, added to an equal volume of ice-cold PBS, and pelleted by centrifugation at 4°C.

Total RNA was isolated from cell pellets as described previously (45) using an RNeasy Kit (Qiagen) and DNA removal was performed using a TURBO DNA-free kit (Ambion). DNA removal was confirmed by PCR using OL398 and OL399. Sample quality was assessed using an Agilent 2100 Bioanalyzer system and corresponding RNA 6000 Nano kit (Agilent) to confirm RNA integrity. Samples with a RIN of $\geq$9.9 were used in this study. Prior to mRNA enrichment, biological triplicates were pooled at equal RNA concentrations. rRNA was then removed using a Ribo-Zero Kit for Gram Negative Bacteria (Illumina) followed by a MICROBExpress Bacterial mRNA enrichment kit (Agilent). Removal efficiency of rRNA was confirmed using an Agilent 2100 Bioanalyzer system and RNA 6000 Nano kit (Agilent). Enriched mRNA samples were then used for RNA sequencing using an Illumina NextSeq. Library preparation and RNA sequencing was performed following Truseq Stranded mRNA Kit (Illumina) recommendations omitting mRNA enrichment steps. Quality, concentration, and average fragment size of each sample was assessed using an Agilent 2100 Bioanalyzer system and RNA 6000 Nano kit (Agilent) prior to sequencing. Library concentration for pooling of barcoded samples was assessed by RT-qPCR with a KAPA Library Quantification kit (KAPA Biosystems) as recommended for high sensitivity. Samples were run on an Illumina NextSeq with a corresponding 150-cycle NextSeq Mid Output Kit v2.5. Experimental data from this study were deposited in the NCBI Gene Expression Omnibus (GEO) database (GEO accession numbers GSE164233 and GSE164290).

RNAseq bioinformatics: Data was exported from BaseSpace (Illumina) in fastq format and analyzed using CLC Genomics Workbench 20 (Qiagen Bioinformatics). Reads were imported and failed reads were removed using the Illumina Paired Importer tool, with quality score parameter option set to Illumina Pipelines 1.8 and later. The total number of reads generated for each sample was at least 15.49 million and up to 22.22 million, resulting in ≥545x read coverage for each sample. Reads corresponding to rRNA were filtered, removed by aligning to known rRNA sequences, and discarded. Samples contained between 0.27% and 0.71% rRNA. Remaining read sequences were aligned using the RNA-seq Analysis tool (v0.1) with default parameters and defined strand specificity to the *A. baumannii* AB5075 NCBI reference genome (CP008706.1). Gene expression values were calculated using the Expression Browser tool (v1.1) specifying transcripts per million (TPM) as the output. Differential expression values between samples were generated using the Differential Expression in Two Groups tool (v1.1) for whole transcriptome RNA-seq samples. Differential expression is reported as fold-change of expression for biofilm relative to planktonic samples, and cspC mutant relative to wildtype samples. Library size normalization is automatically performed using the trimmed mean of M values (TMM) method by the Differential Expression in Two Groups tool (46). Ontology classification of genes was assigned based on the Kyoto Encyclopedia of Genes and Genome (KEGG) (47). Genomes and differential expression visualizations (Fig. 1A and 5A) were generated using Circos (48).

RT-qPCR transcriptional analysis: To validate RNA-seq findings, a selection of genes were assayed by Real-Time Quantitative Reverse Transcription PCR (RT-qPCR). Strains were grown and RNA harvested as described above for RNA-seq studies performed on biofilm and planktonic samples in biological triplicate. Total RNA was isolated from cell pellets and DNA removal was performed as described above. Sample quality was assessed using an Agilent 2100 Bioanalyzer system and corresponding RNA 6000 Nano kit (Agilent) to determine RNA concentration and to confirm RNA integrity. Samples with a RIN of $\geq$9.9 were used. One microgram from each sample was reverse transcribed using an iScript cDNA Synthesis Kit (BioRad). RT-qPCR was then performed using gene-specific primers (Table S1) and TB Green Premix Ex Taq (Takara). Levels of gene expression were normalized to that of 16S ribosomal RNA gene (OL4498 and OL4449) and fold-change of expression was assessed for biofilm relative to planktonic samples, and cspC mutant relative to wildtype samples, using the $2^{-\Delta\Delta Ct}$ method (49).

Similarly, transcriptional analysis was used to assess changes in *cspC* transcript levels under cold stress. *A. baumannii* wildtype cultures were grown overnight as described above, in biological triplicate, and sub-cultured into 5 mL of fresh media. After 3 hours of growth at 37°C, new 5 mL cultures were seeded and standardized to and OD_{600} of 0.05. Bacteria were transitioned to 15°C for 15 minutes to induce cold shock, and control samples were left at 37°C. Following this, samples were combined with an equal volume of ice-cold PBS and pelleted by centrifugation at 4°C. Total RNA isolation, DNA removal, and reverse transcription were performed as described above. Quantitative,

real-time RT-PCR (qRT-PCR) was then performed using *cspC*-specific primers OL5216 and OL5217, and TB Green Premix Ex Taq (Takara). Levels of gene expression were normalized to that of 16S ribosomal RNA gene (OL4498 and OL4449) and fold-change of expression was assessed for cold shocked samples relative to non-cold shocked samples using the $2^{-\Delta\Delta Ct}$ method (49).

Crystal violet and real-time biofilm assays: *A. baumannii* biofilm formation was performed as described above in biological triplicate. After 24 hours of static growth, biofilms were washed 3 times with PBS and fixed with 100 μL of 100% ethanol. After drying, 200 μL of crystal violet was added, incubated at room temperature for 15 minutes, and biofilms washed 3 times with PBS. After a second drying step, 100 μL of 100% ethanol was added to solubilize the crystal violet. Absorbance of solubilized crystal violet was measured at OD_{543} and reported as percent variance to that of the wildtype strain.

A Real Time Cell Analyzer (RCTA) xCELLigence MP (ADCEA Bioscience) instrument was used to monitor biofilm formation over time. The xCELLigence RTCA MP was placed in a 37°C incubator for one hour prior to experimentation to allow the instrument temperature to equilibrate. Next, 96-well E-plates were loaded with 180 μL of LB, positioned in the RTCA, and measured for background signal. Using the same plate, *A. baumannii* biofilms were prepared as described above, and statically incubated in the RTCA, with reads taken every 15 minutes for 25 h. The data generated herein is from nine biological replicates per strain.

Microscopy: Cell morphology was assessed by fluorescence microscopy as previously described (50) with minor modifications. Briefly, single 24h wildtype, *cspC::tn* mutant and complemented strain colonies were resuspended in 100 µL of 1x PBS. Cell membranes and DNA was stained with FM4-64 and DAPI, respectively, at final concentrations of 1 µg/mL. Cell suspension (5 µL) were spotted onto a glass coverslip of glass bottom dishes (MatTek) and subsequently covered with a sterile pad of 1% agarose in water. Imaging was completed at room temperature inside a DeltaVision Elite deconvolution fluorescence microscope (GE Applied Precision) environmental chamber. Photos were captured using a CoolSNAP HQ2 camera (Photometrics) and images were acquired by taking 17 z-stacks at 200 nm intervals. All images were deconvolved using the softWoRx (GE Applied Precision) imaging software.

Extracellular DNA assays: Extracellular DNA production of *A. baumannii* biofilms was analyzed quantitatively as described previously (51). Briefly, *A. baumannii* biofilm formation was initiated as described above in biological triplicate. After 24 hours of growth, supernatant was removed, and biofilms were washed once with 200 µL PBS. eDNA in biofilms was quantified by Quant-iT PicoGreen dsDNA labelling (Thermo Fisher) and fluorescence measured using a Synergy2 plate reader (BioTek).

Biofilm inhibition by proteinase K and sodium *meta*-periodate: Disruption of *A. baumannii* biofilms by sodium *meta*-periodate and proteinase K was analyzed

quantitatively as described previously (52). Briefly, *A. baumannii* biofilm formation was initiated as described above in biological triplicate. Biofilms were supplemented with a final concentration of 100, 50, 25, 12.5, 6.25, 3.13, 1.56, 0.78, or 0 mM of sodium *meta*-periodate. Alternatively, biofilms were supplemented with a final concentration of 50 µg/mL of proteinase K. Biofilms were allowed to form for 24 h at 37°C and then quantified by crystal violet assay as described above.

Cold-shock recovery and survival: *A. baumannii* cultures were grown overnight, in biological triplicate, and sub-cultured into 5 mL of fresh media. After 3 hours of growth, new cultures were seeded and standardized to and OD_{600} of 0.05. For cold stress recovery, after one hour of growth at 37°C bacteria were transitioned to 15°C for 1 hour. Following this cold stress, bacteria were returned to 37°C with shaking. Bacteria were plated on TSA every hour to determine CFU/mL as a measure of recovery rate. Alternatively, for cold stress survival, bacteria were immediately placed at 15°C after culture standardization and plated on TSA every hour to determine CFU/mL for monitoring survival.

Antibiotic susceptibility assays: Antibiotic sensitivity was assessed by performing minimum inhibitory concentration (MIC) assays as previously described (53). Briefly, *A. baumannii* strains were grown in LB overnight, in biological triplicate, at 37°C with shaking. Overnight cultures were diluted 1:1,000 with fresh LB and 195 µL was added to 96-well microtiter plates. Subsequently, antibiotics were serial diluted and 5 µL of each concentration, or solvent (no-treatment control), was added. Antibiotic solvents were as

follows: ciprofloxacin, 0.1M NaOH; chloramphenicol, 70% EtOH; streptomycin, H_2O; gentamicin, 100% EtOH; kanamycin, H_2O; neomycin, H_2O; Fosfomycin, H_2O; oxacillin, H_2O. Cultures were grown overnight at 37°C with shaking. MIC is reported as the lowest antibiotic concentration resulting in inhibition of growth compared to no-treatment control.

CspC protein architecture analysis: Domain and motif scanning was performed using ScanProsite (54) with the amino acid protein sequence of CspC (GenBank: AKA31122.1) as the input. The alignment of 207 UniProtKB/Swiss-Prot sequences of true positive hits for the detected cold shock domain profile (PS51857) were retrieved and a sequence logo was generated from this alignment on Prosite. Three-dimensional protein modeling via homology modelling was completed using Swiss-Model (55). The Swiss-Model template library contained 244 templates matching the CspC amino acid sequence, with the most closely related, and the sequence with the highest global model quality estimate, being CspA of *Escherichia coli* (56).

Transcriptional arrest and determination of mRNA half-life: Determination of RNA half-life was performed as described previously with minor modifications (57). Six biological replicates of *A. baumannii* cultures were grown overnight and sub-cultured into 5 mL of fresh media. After 3 hours of growth, new cultures were seeded and standardized to and OD_{600} of 0.05 in 100 mL of fresh LB. After 3 h of growth to reach exponential phase, and prior to transcriptional arrest, 5 mL of each culture was collected, immediately combined with 5 mL of ice-cold PBS, and pelleted by refrigerated centrifugation (t=0). Rifampin at a final concentration of 250 µg/mL was then added to

bacterial cultures. At 5, 10, 15, 30, and 45 minutes post-treatment, 5 mL of each sample was collected, immediately combined with 5 mL of ice-cold PBS, and pelleted by refrigerated centrifugation. Immediately following each refrigerated centrifugation step, supernatant was removed and cell pellets were stored at -80°C. Total RNA extraction, confirmation of RNA quality, and RT-qPCR was performed as described above for each sample (primers used are listed in Table S1). RNA abundance at each timepoint post-treatment was calculated for each biological replicate and measured in technical triplicate for each timepoint using $2^{-\Delta\Delta CT}$ relative to initial RNA abundance (t=0). These values were plotted as a function of time and an exponential, one phase decay curve was fitted using GraphPad Prism. The decay curve is represented as $R(t) = R_0e^{-kt}$, where R_0 and $R(t)$ are relative RNA abundance at initial and subsequent timepoints, respectively (58). The decay rate constant, k, is equal to $\ln(2)/t_{1/2}$, where $t_{1/2}$ is mRNA half-life. Accordingly, half-life was derived from this equation as $t_{1/2} = \ln(2)/k$.

RNA secondary structure predictions: RNA secondary structure predictions were generated using RNAfold (ViennaRNA package v2.4.18) using default parameters (59). Full length mRNA sequences, as revealed by RNA-seq read mapping, were used as input. All structures predicted by RNAfold were inspected and compared. Consensus structures with the lowest minimum free energy were downloaded in Vienna format and used to draw RNA structure using the forna software (ViennaRNA package v2.4.18) (60).

Human blood survival assay: Survival in whole human blood was performed as previously described (61) with minor modifications. Briefly, *A. baumannii* cultures were grown overnight, in biological triplicate, and sub-cultured into 5 mL of fresh LB. After 3 hours of growth, 10 mL of cells were centrifuged, washed with PBS, and diluted to an OD_{600} of 0.5. Cells were then added to 1 mL of deidentified whole human blood (BioIVT) at a final OD_{600} of 0.05. The initial inoculum of each strain was determined at this time by serial dilution and plating on LB agar. Blood cultures were incubated at 37 °C with agitation, and CFU/mL of each strain was determined, every hour for six hours, by serial dilution and plating on LB agar.

Oxidative stress assay: Oxidative stress was assessed using hydrogen peroxide as described previously (62) with minor modifications. Briefly, *A. baumannii* cultures were grown overnight in biological triplicate and sub-cultured into 5 mL of fresh media. After 3 hours of growth, new cultures were seeded and standardized to and OD_{600} of 0.05 in fresh LB. Hydrogen peroxide was then added to the cell suspensions for a final concentration of 2 mM and grown at 37°C with agitation. Cells were collected (500 µL) at each indicated timepoint and supplemented with catalase (10 µg/mL) to neutralize the effects of hydrogen peroxide. Cells were then serial diluted and plated on LB agar to determine surviving CFU/mL.

Mouse infection model: The experiments were performed with the prior approval of the University of South Florida Institutional Animal Care and Use Committee. A murine model of dissemination was performed based on previous studies (63, 64). Briefly, 13-

week-old, female BL-6 mice were purchased from Charles River Laboratories and allowed to acclimate for 2 weeks prior to the start of experimentation. AB5075 wild-type and *csp::tn* strains were grown in LB as described above in biological triplicate. Overnight cultures were then sub-cultured 1:100 in fresh LB and grown for an additional 3 hours. Cultures were then pelleted by centrifugation, washed twice in PBS, and standardized to an OD_{600} of 5.0. From this resuspension, the average number of CFU/mL was calculated for each strain by plating on LB agar. This was repeated on three separate days using two biological replicates per strain, and the average number of CFU/mL across replicates was calculated for each strain. This average number of CFU/mL was used to determine the volume of bacteria needed to obtain a 5-mL inoculum of 2.5×10^8 ([2.5×10^8/average CFU/mL] × 5 mL). On the day of infection, appropriate aliquots from fresh overnight cultures were prepared in the same manner, diluted to 2.5×10^8 CFU/mL, and 100 µL of suspension was administered to 10 mice per strain via retroorbital injection, providing a final inoculum of 2.5×10^7 CFU/mL. Infections were monitored and the mice were sacrificed 6 hours post infection. At this time, whole liver, heart, kidneys, spleen, lungs, and brain were harvested and immediately stored at −80°C. Organs were individually homogenized using a Bullet Blender (Next Advance) in 1.5 mL PBS and serially diluted onto LB agar to determine bacterial burden (CFU/mL). A Mann-Whitney nonparametric test was performed to determine statistical significance of bacterial burden for each organ between the mutant and wild-type strains.

Results

Identification of *A. baumannii* biofilm-associated genes: To inform on factors potentially important to biofilm formation, global gene expression within AB5075 wild type biofilm populations was compared to planktonic counterparts (Fig. 1A, Table S2). Of the genes differentially expressed by a magnitude ≥2-fold, 352 genes were expressed higher in biofilm cell populations (Fig. 1B), whilst just 86 genes were enriched ≥2-fold within planktonic cells.

When sorted ontologically, most biofilm-associated transcripts were categorized within the genetic regulation group; fulfilling roles pertaining to DNA replication, transcriptional regulation, and translation (Fig. 1C). Of the 58 genes within this cluster, 27 are annotated as transcription factors. Furthermore, an overwhelming 25 of these transcription factors were enriched in the biofilm population. The *A. baumannii* strain AB5075 genome encodes for 243 transcription factors (65); indicating 10% of known transcription factors are activated in biofilms, with 1% deactivated, suggesting a distinct global regulatory response within this population. Of the 25 biofilm-associated transcription factors, the majority (n=23) are conserved among *A. baumannii* strains, with one, ferric uptake regulator *fur*, having been previously deemed essential for growth in rich medium (37, 66). Of the two less-conserved regulators, HTH_3 family transcriptional regulator, *ABUW_RS16125,* was previously shown to be essential for survival during *Galleria mellonella* infection (67). This may suggest a dual virulence and biofilm enhancing role for ABUW_RS16125 in *A. baumannii* strains encoding this gene.

The upregulation of a cadre of genes involved in metabolic pathways was also apparent within biofilms. The most drastically enriched transcripts were those responsible for energy metabolism, and specifically the sulfur metabolism pathway (68). This included genes encoding for subunits of the taurine transporter permease (*tauA, tauB,* and *tauC*), taurine dioxygenase (*tauD*), sulfate transporter permeases (*cysT, cysW*), and thiosulfate-binding protein (*ABUW_RS05010*), each of which showed ≥7.69-fold enrichment. Several additional genes involved in the sulfur metabolism pathway were also upregulated by ≥2-fold in biofilms, including sulfate transporter permease (*ABUW_RS04990*), thiosulfate-binding protein (*ABUW_RS01375*), and sulfate adenylyl transferase subunits (*cysN* and *cysD*).

Six genes identified as contributors to antimicrobial drug resistance and disease were also upregulated in biofilm. This group included *ABUW_RS09485* and *ABUW_RS09480*, which encode a putative efflux pump and its accompanying membrane fusion protein component, respectively, and are homologous to the *E. coli* efflux pump, EmrAB. Other ontologies with altered expression in biofilms included additional membrane transporters (e.g. – *ABUW_RS11790, ABUW_RS11795, ABUW_RS18795*) and putative membrane proteins (e.g. – *ABUW_RS10540, ABUW_RS17095, ABUW_RS18900*); carbohydrate metabolism (e.g. – *ABUW_RS08155, leuA, ABUW_RS10665*); and amino acid metabolism (e.g. – *yncA, ABUW_RS13045, mmsB*). Thus, it is clear that the biofilm has unique regulatory

423 networks activated compared to that of planktonic cells, which reflect distinct metabolic
424 needs and response to the environment.
425
426 To validate RNA-seq findings, a selection of genes were assayed by Real-Time
427 Quantitative Reverse Transcription PCR (RT-qPCR), with fold-change in expression
428 proving comparable to RNA-seq findings (Fig. S1).
429
430 **Physiological impact of biofilm-associated genes on biofilm integrity:** Preferential
431 expression within biofilm populations does not necessary indicate that a given gene
432 product has a role in biofilm formation. Thus, to explore genes with a tangible role in
433 biofilm formation, we first narrowed the list of 352 genes with biofilm-enriched
434 transcripts to those meeting the following criteria: confident read coverage (>85%
435 uniquely mapped reads), relatively strong expression (TPM $\geq$115 in biofilm), and
436 greatest fold-increase (>3-fold) (Table 2). Of the genes fitting this criteria, the most
437 highly expressed gene was *ssrS* (62175.62 TPM), which produces the well-conserved,
438 6S RNA (69); whilst the most upregulated gene within biofilms compared to planktonic
439 populations was *ABUW_RS05005* (+60.17-fold), which encodes an uncharacterized
440 alpha/beta hydrolase fold protein. We next assessed whether the 40 genes within these
441 parameters have an impact on biofilm formation by performing classic crystal violet
442 biofilm assays on transposon mutants for the genes of interest contained within the
443 University of Washington *A. baumannii* AB5075 transposon mutant library (37). In so
444 doing, we uncovered 24 genes whose disruption led to reduced biofilm formation (Fig.
445 2). Of these, 17 mutant strains showed >50% reduction in biofilm. The largest changes

were observed for *ABUW_RS09460* and *ABUW_RS05005,* with >72% reduction in biofilm mass for their respective mutant strains. Although both *ABUW_RS09460* and *ABUW_RS05005* mutants show comparable reduction in biofilm mass, *ABUW_RS09460* was only modestly upregulated (3.07-fold), whereas *ABUW_RS05005* was markedly upregulated (60.17-fold) in biofilm. Significant changes in biofilm formation were also observed for *cspC*, and *hscB* mutants (>40% reduction), with *cspC* being the highest expressed gene (1324.94 TPM), whilst *hscB* was one of the lowest expressed genes (167.95 TPM) within biofilms investigated in these assays. Altogether, neither fold-change in expression nor magnitude of expression exclusively correlate with physiological impact on biofilm formation, but rather each feature must be considered holistically.

To assess whether the observed changes in biofilm production may be due to a growth defect in the mutant strains, we measured cell density over time in liquid culture compared to wildtype (Fig. S2A). In so doing we noted that the vast majority of mutants behaved just as the wildtype, with only a handful of strains exhibiting growth defects. These included the transposon mutant for *csp1*, which grew in a similar manner to the parent for the first 3h, but then essentially plateaued in growth, reaching a maximum cell density (OD_{600}) of 0.883±0.014 at 8.5 h (WT OD_{600} = 1.133±0.006 at 11.5 h). Another strain with a notable growth defect was the *tauA* mutant, which exhibited a less pronounced exponential growth phase, reaching a cell density of 0.602±0.011 by 4 h (WT OD_{600} = 0.769±0.018 by 4 h). The remaining mutant strains grew at rates comparable to wildtype and reached similar, if not higher, maximum cell densities. This

469 indicates that the observed reduction in biofilm formation is unlikely to be an artifact of
470 poor growth, with the exception of the *csp1* and *tauA* mutant strains.
471
472 **Disruption of *cspC* leads to changes in colony morphology and biofilm EPS:**
473 During our screen, we noted that one particular mutant, *cspC::tn* (+3.2-fold transcription
474 in biofilm), produced a mucoidal, non-mucoviscous phenotype when grown on LB agar
475 (Fig. 3). The *cspC* gene was one of the highest expressed genes within the biofilm
476 (1324.94 TPM) and encodes a putative cold-shock protein, the role of which has not
477 been previously characterized in *A. baumannii.* Importantly, complementation of *cspC in*
478 *trans* restored colony morphology and biofilm production levels to those comparable to
479 wildtype (Fig. 3 and 4A), and no measurable differences in growth (Fig. S2B). When
480 observing *cspC* mutant cells by fluorescence microscopy, cell morphology was
481 unaltered with respect to shape, size, and chaining (Fig. S3), indicating that obvious
482 morphological differences are unlikely to contribute to the phenotype observed.
483
484 To gain insight as to how and when CspC impacts biofilm formation, we used an
485 xCELLigence RTCA to track biofilm formation in real time. The RTCA measures biofilm
486 progression based on impedance of electrical signals between electrodes lining each
487 well of a specialized 96-well plate, and expresses these measurements as a relative
488 unit cell index (CI). CI measurements are influenced by cell adherence, secretion of
489 extracellular polymeric substance (EPS), and cell spreading (70, 71). When CI values
490 reach their maximum and remain steady, this signifies that the biofilm has entered
491 maturation (70). In agreement with our crystal violet studies, the rate of increase and

overall maximum CI value reached was noticeably lessened for the *cspC* mutant strain when compared to the parent and complement strains (Fig. 4B).

As cold-shock proteins have demonstrated importance in cell aggregation (31), extracellular polysaccharide production, and membrane fluidity (32), we hypothesized that the altered cellular morphology and decreased CI values of the *cspC* mutant may be due to changes in EPS production. Indeed, upon testing, we noted that *cspC* mutant biofilms showed increased tolerance to polysaccharide degradation by sodium *meta*-periodate compared to the wild type and complement strains (Fig. 4C). Conversely, the *cspC* mutant biofilm contained a comparable amount of eDNA to wildtype; and when we performed biofilm profiling assays in the presence of proteinase K, no change in biofilm integrity was observed (Fig. S4) suggesting that protein and eDNA components are not contributing to the biofilm defect observed upon *cspC* disruption.

***cspC* is induced under cold-shock conditions but does not impact cold shock survival:** CspC bares the same domain architecture as classic cold-shock proteins, which are defined as nucleic acid-binding proteins that are induced during temperature downshifts (34). To explore whether this is true of *cspC*, its transcription was measured during cold stress. Upon analysis we observed that *cspC* transcript levels were moderately increased compared to expression at 37°C (Fig. S5A) by approximately 1.5-fold. When the *cspC* mutant was challenged with cold stress for 1 hour, however, we did not observe any impact on cell viability (Fig. S5B). Furthermore, the *cspC* mutant also did not exhibit impaired survival during sustained cold stress (Fig. S5C). It is noteworthy

that the *cspC* transcript is relatively abundant at 37°C, in both biofilm (1324.94 TPM) and planktonic conditions (408.71 TPM). Active transcription under varied conditions, coupled with the apparent lack of impact during cold stress, suggests that the role of CspC may extend beyond cold adaptation in *A. baumannii*.

Transcriptional regulation by CspC: Csps are multifunctional proteins that can wield impacts at the level of transcription, post-transcription, and translation (reviewed in (34, 35)). How they exert their pleiotropic effects is either as a transcriptional regulator or RNA chaperone (33). To inform on the mechanism(s) governing the observed physiological changes upon *cspC* disruption in *A. baumannii*, we performed RNA-seq with our mutant and wild-type strains (Fig. 5A, Table S3). In so doing, we observed 147 genes upregulated and 54 genes downregulated by $\geq$2-fold upon *cspC* disruption (Fig. 5B). When sorted ontologically, it is apparent that a large portion of upregulated transcripts pertained to phage-related genes within the same chromosomal locus (n = 49) (Fig. 5C). Of these, 31 fall within the region predicted to encode Acinetobacter phage Bϕ-B1251, and the remaining 17 are within Ab105-1ϕ. Recent work has identified these regions as encoding active *Siphoviridae*- and *Myoviridae*- family phages, respectively, and as the two most prevalent phages identified among *A. baumannii* genomes (72).

A notable trend of opposing regulation of membrane transporter proteins compared to non-transporter membrane proteins was also apparent in our dataset. All 8 differentially expressed membrane protein genes, with no transport function, were downregulated,

538 including type 1 pili subunits *csuAB* (6.19-fold) and *csuC* (2.7-fold), and fimbrial subunit,
539 *fimA* (3.28-fold), each of which is important for attachment of *A. baumannii* to abiotic
540 surfaces (24, 26, 73). Of the differentially expressed membrane transporters, 8 of 10
541 showed increased transcription, including *adeFG* (≥4.78-fold), which encode
542 components of multi-drug efflux pumps. Also upregulated were the accompanying
543 component *adeH* (3.29-fold) and additional efflux pump genes, *adeIJ* (≥2.08-fold) and
544 *abeS (ABUW_RS06550*, 2.43-fold), which were categorized separately under
545 Antimicrobial Drug Resistance by KEGG ontology. The AdeFGH efflux pump has been
546 reported to confer resistance to DNA damaging agents and chloramphenicol, among
547 other antimicrobials (74), and its overexpression has been correlated to increased
548 biofilm formation of *A. baumannii* clinical isolates, by potentially serving a role in
549 quorum-sensing (75). Like *adeFGH*, *adeIJK* and *abeS* encode components of multi-
550 drug efflux pumps known to confer antimicrobial resistance in *A. baumannii* (74, 76, 77).
551 Overexpression of *adeFGH* and *adeIJK* has previously been shown to decrease
552 production of biofilm in *A. baumannii*, and for *adeIJK* overexpressing mutants, this has
553 been attributed to decreased CsuAB, CsuC, and FimA abundance (78).
554
555 Other ontologies with enhanced expression in the *cspC* mutant included amino acid
556 metabolism (e.g. – *pepD, glyA*); regulatory factors (e.g. – *rpoH, adeL,*
557 *ABUW_RS06565*); and carbohydrate metabolism (e.g. – *gapN, atoA, atoD*).
558 Collectively, it is clear that cspC has a global impact on the transcriptional homeostasis
559 of *A. baumannii* and acts to regulate factors with many and varied roles within the cell.
560

To validate RNA-seq findings, a selection of genes were assayed by Real-Time Quantitative Reverse Transcription PCR (RT-qPCR). Trends in differential expression within the *cspC* mutant relative to wildtype were comparable to that of RNA-seq findings (Fig. S6).

CspC influences the antimicrobial resistance profile of *A. baumannii*: Previous work employing a spontaneous mutation screen identified *cspC* as one of several genes able to restore, at least in part, antibiotic resistance in an AB5075 *bfmRS*-null strain (79). Considering this, and the upregulation of multi-drug efflux pump components observed in our study, we hypothesized that the *cspC* mutant would display phenotypic antibiotic tolerance. Indeed, previous work has shown that the AdeIJK efflux system (strongly upregulated in the *cspC* mutant) contributes to resistance towards a wide range of substrates including β-lactams, chloramphenicol, ciprofloxacin, and, in part, aminoglycosides (76, 80). Accordingly, we conducted an MIC screening panel for the *cspC* mutant using a variety of antimicrobial agents. In so doing we noted that disruption of *cspC* resulted in increased tolerance to ciprofloxacin, chloramphenicol, and streptomycin, yet slightly increased sensitivity to gentamicin, kanamycin, neomycin and fosfomycin (Table 3). Previous studies have demonstrated a strong correlation between *adeIJK* expression and ciprofloxacin resistance, with *adeIJK* overexpression mutants exhibiting enhanced resistance and *adeIJK* null strains demonstrating sensitivity; a phenomenon that is conserved across *A. baumannii* strains (74, 76, 78, 81, 82). Similarly, for multiple strains, transcription levels of *adeFGH* and *adeIJK* correlates with chloramphenicol resistance, with *adeFGH* transcription having the greatest influence

(74, 76, 78). Thus, it seems possible that the upregulation of *adeIJK* in the *cspC* mutant is contributing to the measurable increase in ciprofloxacin tolerance, and similarly, the upregulation of both *adeIJK* and *adeFGH* may be contributing to enhanced chloramphenicol resistance. The disruption of *cspC* also resulted in slightly higher sensitivity to the majority of aminoglycosides tested (gentamicin, kanamycin, neomycin). Deletion of *adeABC* and *adeIJK* has been shown to induce gentamicin sensitivity, with *adeABC* deletion having significantly greater impact (78, 81, 82). In agreement with this, previous work has demonstrated that overexpression of *adeABC,* but not *adeFGH* nor *adeIJK*, enhances gentamicin, kanamycin, and neomycin resistance (78). Considering this, and that the *cspC* mutant has elevated *adeFGH* and *adeIJK* expression, but unchanged *adeABC* expression, the increased sensitivity to aminoglycosides is likely not attributed to these efflux pumps.

CspC regulates mRNA stability of transcriptional regulators *adeL* and *ABUW_RS06565*: When bacteria experience temperature downshifts, single-stranded DNA and RNA secondary structures are consequently stabilized. This leads to inhibited transcription and/or translation and RNA degradation, which adversely effects cellular function. Csps possess a conserved nucleic acid-binding domain that allows them to bind single-stranded DNA and RNA, and rescue undesirable secondary structures. Specifically, this nucleic acid-binding domain is typically comprised of a ribonucleoprotein (RNP)-1 and RNP-2 motif, which facilitates interaction with nucleic acids and has chaperone activity (34). When interrogating the amino acid sequence of CspC, a conserved cold shock domain signature was apparent (Fig. S7). This domain

607 contains both a RNP-1 and RNP-2 motif (Fig. 6A). Structural prediction of CspC
608 revealed that these motifs are both within the β2 and β3 strands of the antiparallel β-
609 barrel structure (Fig. 6B). This arrangement makes the RNP motifs spatially available
610 for binding to ssDNA and RNA, as is the hallmark characteristic of Csps (83, 84).
611
612 In order to determine if CspC may function as an RNA chaperone for the identified
613 differentially expressed targets, we assessed the impact of *cspC* mutation on the rate of
614 decay for putative target mRNAs. To do so, cells were grown to exponential phase and
615 treated with rifampin to inhibit transcription. RNA was then isolated from wildtype and
616 *cspC* mutant strains at consecutive time points post-transcriptional arrest. Using RT-
617 qPCR, we assessed RNA transcript levels at each timepoint and determined decay rate
618 by plotting the change in transcript abundance relative to transcript level immediately
619 prior to rifampin treatment. The close arrangement of efflux pump encoding genes
620 *adeFGH* indicates that these genes are likely within an operon, and similar conclusions
621 can be drawn for *adeIJK*. Further supporting this, RNA-seq read alignments (data not
622 shown) revealed transcript readthrough between the individual genes of each efflux
623 pump. Considering this, we selected *adeG* and *adeJ,* located in the middle of their
624 respective operons, for mRNA half-life studies. The half-life of *adeJ* mRNA was slightly
625 longer than that of *adeG* (Fig. S8, Table 4) in the wild-type strain, however half-lives for
626 both transcripts were comparable between the parents and *cspC* deficient strains. This
627 suggests that CspC has no impact on the stability of *adeJ* and *adeG* mRNA.
628 Importantly, the half-life of *recA* was also tested, and found to be 4.674 minutes in

629 wildtype, which is comparable to the previously determined half-life of 4.5 minutes (57),
630 indicating that the experimental approach used herein is reproducible.
631
632 Considering that the half-lives of the major efflux pump transcripts were unaffected, we
633 next considered whether CspC could be acting as an mRNA chaperone for
634 transcriptional regulators. Transcription of *adeFGH* is repressed by the LysR type
635 transcriptional regulator *adeL* (upregulated +2.8-fold in the *cspC* mutant, Table S3, Fig.
636 S6), located immediately upstream of the *adeFGH* operon (74). When assessed
637 experimentally, we found that the half-life of *adeL* was increased in our mutant from
638 1.28 minutes in the parent to 2.54 minutes in the *cspC*$^{-}$ strain (Fig. 7A, Table 4). Further
639 to this, we also investigated the half-life of *ABUW_RS06565,* an uncharacterized GntR
640 family transcriptional regulator*,* which was upregulated 2.98-fold in the *cspC* mutant.
641 *ABUW_RS06565* was the only transcriptional regulator with altered transcription, aside
642 from *adeL,* that was not part of the collectively altered Bϕ-B1251 and Ab105-1ϕ phage
643 loci genes. The half-life of *ABUW_RS06565* rose from 1.75 minutes in the wild-type
644 strain to 2.57 minutes in the mutant – a 1.5-fold increase in the *cspC* mutant compared
645 to the parent (Fig. 7B, Table 4). This indicates that the mRNAs of transcriptional
646 regulators *adeL* and *ABUW_RS06565* are in fact more stable as a result of *cspC*
647 disruption.
648
649 The average mRNA half-life varies depending on bacterial species and growth
650 condition, however, the average RNA half-life hovers between 2-5 minutes (85-88).
651 Considering this scale, the extended half-lives of *adeL* and *ABUW_RS06565* RNA in

the *cspC* mutant are likely substantial. It is important to note that increased half-life of *adeL* does not necessarily indicate enhanced AdeL repression of *adeFGH*. Csps have the ability to destabilize RNA secondary structures in order to liberate the RBS and permit translation (reviewed in (35)), therefore, the absence of CspC could cause enhanced *adeL* stability resulting in increased transcription, but abrogated translation. In support of this notion, RNA secondary structure prediction revealed a stable hairpin formed in the 5'UTR of *adeL,* immediately upstream of a putative AGGAG ribosomal binding site (RBS) (Fig. 8). This is of particular interest as previous studies measuring mRNA half-lives in *E. coli* determined that an AGGAG motif in 5′UTRs, specifically within 2 to 8 nucleotides of translational start codons, is frequently found in transcripts with enhanced stability compared to the global mRNA population (89). The *ABUW_RS06565* transcript presents a curiosity as an obvious RBS is not apparent, however a similar, stable 5'UTR structure is also evident. Additionally, the *ABUW_RS06565* transcript contains an unusual, A/T-rich region beginning at the 5th codon. A/T-rich sequences within RNA, particularly from the 5th to 8th codon of a protein coding region, have been shown to significantly enhance translation initiation in *E. coli.* This suggests that the inaccessibility of this motif due to enhanced RNA stability may also impede translation initiation of this transcription factor upon *cspC* deletion (90).

CspC is required for survival during oxidative stress and challenge by components of the human immune system: Biofilm production contributes to bacterial survival against host immune responses (91), and previous studies have found that a majority of *A. baumannii* bloodstream isolates are capable of producing robust

biofilms (92). Furthermore, altering the balance of attachment, growth, and dispersal of a biofilm results in negative impacts on the capacity to cause bloodstream infections (93). Given that the *cspC* mutant has decreased propensity for biofilm formation, we speculated that the loss of CspC would impact *A. baumannii* survival in human blood. Thus, we grew the wild-type, mutant and complement strains in whole human blood for 6 h. Upon analysis we noted that AB5075 cell viability declined 67.6% from 0-1h, followed by an increase in viability as time progresses (Fig. 9A). In contrast, the *cspC* mutant strain fared markedly worse, demonstrating a far more severe decline in cell viability from 0-1h (86.6%), with cell viability counts remaining relatively stagnant as infections progressed. As expected, the *cspC* complement strain had a similar survival capacity as the wild type, indicating a clear requirement for CspC for survival during *A. baumannii* engagement with human blood.

Bacterial clearance in human blood is mediated by a number of factors, including cell mediated immunity. A primary killing mechanism of leukocytes during engagement with bacterial pathogens is wielded through reactive oxygen species (ROS). It has been previously demonstrated that clearance of *A. baumannii* is dependent on host reduction of nicotinamide adenine dinucleotide phosphate (NADPH) oxidase and subsequent accumulation of ROS (94, 95). Considering this, we hypothesized that the *cspC* mutant would likely have a survival defect upon exposure to oxidative stress, and thus performed a hydrogen peroxide killing assay (Fig. 9B). Upon analysis, we noted that the viability of all strains declined after 10 minutes of exposure to 2 mM hydrogen peroxide, which is a clear indication that the cells are experiencing oxidative stress. At conclusion

of these studies (25 minutes) we observed a comparable number of viable cells were recoverable for the wildtype and complement strains. Conversely, the *cspC* mutant showed no cell recovery beyond 10 minutes of exposure, which indicates that CspC has a major role in bacterial survival for *A. baumannii* in the presence of ROS.

CspC plays a pivotal role during *A. baumannii* systemic infections: Given our findings regarding the ability of the *cspC* mutant to survive challenge by components of the human immune system and reactive oxygen species, we next considered whether it's survival during *in vivo* infection would be impaired. Accordingly, using a murine model of infection, we compared the pathogenic potential of the *cspC* mutant to wild-type AB5075. When assessing mortality, we observed no apparent differences between the strains (data not shown), however, when comparing dissemination of infection, bacterial load was substantially reduced for the *cspC* mutant strain in all organs evaluated (Fig. 10). The most significant reduction observed was for that of the liver, which showed a 43-fold reduction in bacterial load compared to wild type. Although not quite as striking, reduced dissemination of the *cspC* mutant to the other organs was equally remarkable (spleen: 12.16-fold; brain: 6.58-fold; lungs: 5.62-fold; kidneys: 4.32-fold, heart: 3.14-fold). These findings support CspC as a novel regulator of virulence, proving critical for *A. baumannii* survival when challenged by the host innate immune response.

Discussion

In this study we investigated the global transcriptional regulation occurring within biofilms formed by *A. baumannii* AB5075. RNA-sequencing revealed a distinct regulatory response within the biofilm, including the upregulation of 10% of all transcription factors identified to date, and the activation of sulfur metabolism pathway gene transcription. The most upregulated gene within biofilms compared to planktonic populations was *ABUW_RS05005* (+60.17-fold), which encodes an uncharacterized alpha/beta hydrolase fold protein co-expressed with the *cys* sulfate transporters (*cysP, cysT, cysW, cysA*). Flanking genes *cysP* and *cysT* were also significantly upregulated within the biofilm (+51.8-fold and +30.66-fold respectively). Microbiosis (0.1-0.3% O_2) has been shown to induce sulfur metabolism gene transcription (96), and with anaerobic regions known to occur within biofilms (97, 98), conditions may be prompting a metabolic shift towards sulfur metabolism in our studies. *SsrS* was the most highly expressed gene within biofilms (62175.62 TPM), which produces the well-conserved, 6S RNA (69). Studies in *E. coli* have demonstrated that 6S RNA accumulates during stationary phase and represses transcription, in turn, enabling cell survival amid nutrient-limiting conditions (99, 100). It is quite possible that nutrient scarcity within the biofilm's dense bacterial community may induce 6S RNA transcription to reorder gene expression circuits to circumvent nutrient limitation.

Among the enriched transcripts within the biofilm, we identified 24 which had significant physiological impact on biofilm integrity. Mutation of the most highly expressed of these

(*cspC*) resulted in pleiotropic impacts on the cell. CspC is one of four known cold shock protein genes in AB5075, none of which have been thoroughly interrogated for physiological function. Interestingly, *cspC* was one of two Csps upregulated during biofilm growth – the other being *csp1* (+15.48-fold). The function of some Csps have been well studied under cold-shock conditions in a variety of organisms (101-103), however, Csps have diverse physiological impacts and Csp-mediated regulatory mechanisms, especially for those induced by non-cold shock conditions, remain poorly understood (reviewed in (33)). CspC transcription was induced under both cold stress and biofilm conditions; however, it did not have an appreciable role during cold shock. In biofilm, CspC seems to regulate extracellular polysaccharide production, as demonstrated by enhanced tolerance of the *cspC* mutant biofilm towards sodium *meta*-periodate. Extracellular protein and eDNA matrix components were unaffected by CspC, which is perhaps unsurprising as *A. baumannii* clinical isolate biofilms are primarily composed of polysaccharides (104). Increased tolerance to polysaccharide degradation may indicate overproduction and/or structural variation of this matrix component. If the former were true, we would anticipate enhanced biofilm production, but this was not the case. We suggest that structural variation, which would render polysaccharides resistant to sodium *meta*-periodate, may be impairing biofilm integrity in the *cspC* mutant. Such a scenario is supported by the observations of others, where altered colony morphology and abrogated biofilm formation as a consequence of polysaccharide modification has been well described for a variety of bacteria (reviewed in (19)).

764 In previous work, spontaneous mutation of *cspC* bypassed antibiotic hypersensitivity
765 and cell morphology defects in a *bfmRS* mutant strain, which was attributed to reduced
766 transcription of the well-known capsule factor - the K locus (79). No transcriptional
767 change for *cspC* was evident in the *bfmS, bfmR,* or *bfmRS* mutant strains (79), and in
768 our work, *bfmRS* transcription was unaffected by *cspC* disruption. Given that mutation
769 of *cspC* is able to bypass sensitivity phenotypes in previous work, and that the *cspC*
770 mutant has enhanced tolerance to polysaccharide degradation, we anticipated
771 upregulation of the K-locus, a major determinant of capsular polysaccharide production
772 in *A. baumannii*. Surprisingly, no measurable changes for any genes within the K locus
773 were observed, indicating CspC may act independently from the capsule biosynthesis
774 factors within the K locus. Instead, our findings suggest that CspC may mediate biofilm
775 formation through regulation of the *csu* pili assembly system and *fimA* fimbrial subunit
776 transcription, both of which have demonstrated roles in the attachment of *A. baumannii*
777 to abiotic surfaces and were downregulated in the *cspC* mutant strain (24, 26, 73). In
778 particular, Csu pili are adhesive organelles that belong to the archaic chaperone-usher
779 pili class, which facilitate strong adherence to hydrophobic plastics, including
780 polypropylene and polyethylene, which are widely used in medical equipment (26) and
781 are indistinguishable from the materials used in this study. The *cspC* mutant also
782 exhibited elevated multi-drug efflux pump component (*adeFGH, adeIJK)* transcription.
783 Overexpression of *adeIJK* has previously been shown to decrease production of
784 CsuAB, CsuC, and FimA, in turn, altering membrane composition and decreasing
785 biofilm formation in *A. baumannii* (78). In addition to biofilm abrogation, we suspect the
786 cooperative activation of *adeFGH* and *adeIJK* may be contributing to enhanced

787 chloramphenicol resistance as their contribution to resisting the effects of this drug has
788 been well documented (74, 76, 78). Similarly, heightened *adeIJK* expression in the
789 *cspC* mutant may be responsible for the marked increased in ciprofloxacin resistance,
790 as studies have demonstrated a strong correlation between *adeIJK* expression and
791 resistance to this particular fluoroquinolone (74, 76, 78, 81, 82). The consequential
792 upregulation of efflux pumps upon *cspC* deletion may explain why antibiotic resistance
793 was restored for the antibiotic-sensitive *bfmRS* mutant strain once *cspC* mutation was
794 introduced in previous work (79).
795
796 Interestingly, transcription of *adeFGH* repressor, *adeL* (74), was also upregulated in the
797 *cspC* mutant. Csps can have impacts at the transcriptional, post-transcriptional, and
798 translational levels (reviewed in (34, 35)) and we suspect CspC is facilitating *adeL*
799 translation and degradation. In support of this model, the putative *adeL* RBS is in close
800 proximity to a stable secondary structure that likely occludes translation initiation; and
801 *adeL* decay was slowed in the *cspC* mutant. CspC may thus bind the *adeL* mRNA,
802 consequently destabilizing its secondary structure, liberating the RBS, and permitting
803 RNA turnover. Under this model, CspC disruption would lead to increased *adeL* mRNA,
804 but reduced AdeL abundance. Such a regulatory mechanism may not be limited to
805 *adeL*, as the uncharacterized transcriptional regulator, *ABUW_RS06565*, also showed
806 increased transcript abundance and a reduced rate of mRNA decay in the *cspC* mutant.
807 *ABUW_RS06565* does not have an obvious RBS, however, its 5'UTR contains a similar
808 stable secondary structure encompassing an A/T rich, translation-enhancing motif (90).

809 It is quite possible that CspC serves a similar role in destabilizing *ABUW_RS06565* to
810 facilitate translation.
811
812 Structural investigation revealed that CspC contains a conserved RNP-1 and RNP-2
813 nucleic acid binding motif, a hallmark characteristic of Csps. Interestingly, the RNP-2
814 motif contains an arginine residue at position 34, where most bacteria contain a serine
815 residue. Furthermore, the RNP-1 and RNP-2 motifs are bridged by six amino acids, as
816 opposed to the usual seven. The shortened motif separation, but not arginine residue
817 substitution, is a common occurrence for all four *A. baumannii* cold shock proteins
818 (CspC, ABUW_RS12225, Csp1, ABUW_RS15360), with ABUW_ RS15360 having the
819 shortest bridge of 4 amino acids. The combination of both abridged RNP motifs and
820 residue substitution in RNP-2, may alter the affinity of CspC to nucleic acid ligands.
821
822 Importantly, biofilm production contributes to bacterial survival against host immune
823 responses and previous studies have found that a majority of *A. baumannii* bloodstream
824 isolates produce strong biofilms (91, 92). Furthermore, altering the balance between
825 attachment, growth, and dispersal of a biofilm reduces the ability to cause bloodstream
826 infections (93). Disruption of *cspC* resulted in impaired survival in human blood likely
827 due to its limited biofilm forming capacity, and inability to endure in the presence of
828 ROS, the manifestation of which is one of the earliest *in vivo* defense mechanisms
829 against *A. baumannii* (67, 68). Likewise, attenuated dissemination of infection was
830 evident for the *cspC* mutant in a murine model, which establishes CspC as a critical *A.*
831 *baumannii* virulence factor.

In summary, this study identifies CspC as having a critical role for biofilm formation, antibiotic resistance, and virulence via regulation of adhesins and multidrug efflux pumps. Additional studies are needed in order to determine if CspC acts as an RNA chaperone, as we have proposed, to modulate translation. Furthermore, this study identified 23 additional genes with substantial influence over *A. baumannii* biofilm, many of which remain uncharacterized and have not been previously implicated with biofilm formation. Future work will seek to understand how these genes contribute to the complex regulatory network governing *A. baumannii* biofilm formation and to assess their potential as therapeutic targets.

Ethics statement: All animal work was performed under the approval of the University of South Florida's Institutional Animal Care and Use Committee (IACUC).

Acknowledgements: This study was supported by grants AI124458 and AI157506 (LNS) from the National Institute of Allergy and Infectious Diseases and GM133617 (PJE) from the National Institute of General Medical Sciences. The funders had no role in study design, data collection and interpretation, or the decision to submit the work for publication. We extend our thanks to the USF Genomics Program Genomics Equipment Core for the use of their facilities for RNA sequencing.

Author contributions: Conceptualization: B.R.T., L.N.S.; investigation: B.R.T., G.D., R.S.B., P.J.E.; methodology: B.R.T, J.L.A; formal analysis: B.R.T.; writing – original draft preparation: B.R.T.; writing – review and editing: B.R.T., L.N.S.; Funding: L.N.S.

Conflicts of interest: The authors declare that there are no conflicts of interest.

References

1. CDC. 2019. Antibiotic Resistance Threats in the United States, 2019. U.S. Department of Health and Human Services C, Antibiotic Resistance Coordination and Strategy Unit, Atlanta, GA.
2. Tacconelli EM, N. 2017. Global Priority List Of Antibiotic-Resistant Bacteria To Guide Research, Discovery, And Development Of New Antibiotics World Health Organization:7.
3. Turton JF, Kaufmann ME, Gill MJ, Pike R, Scott PT, Fishbain J, Craft D, Deye G, Riddell S, Lindler LE, Pitt TL. 2006. Comparison of Acinetobacter baumannii isolates from the United Kingdom and the United States that were associated with repatriated casualties of the Iraq conflict. J Clin Microbiol 44:2630-4.
4. Lolans K, Rice TW, Munoz-Price LS, Quinn JP. 2006. Multicity outbreak of carbapenem-resistant Acinetobacter baumannii isolates producing the carbapenemase OXA-40. Antimicrob Agents Chemother 50:2941-5.
5. Manikal VM, Landman D, Saurina G, Oydna E, Lal H, Quale J. 2000. Endemic carbapenem-resistant Acinetobacter species in Brooklyn, New York: citywide prevalence, interinstitutional spread, and relation to antibiotic usage. Clin Infect Dis 31:101-6.
6. Maragakis LL, Cosgrove SE, Song X, Kim D, Rosenbaum P, Ciesla N, Srinivasan A, Ross T, Carroll K, Perl TM. 2004. An outbreak of multidrug-resistant Acinetobacter baumannii associated with pulsatile lavage wound treatment. JAMA 292:3006-11.
7. Weber DJ, Anderson D, Rutala WA. 2013. The role of the surface environment in healthcare-associated infections. Curr Opin Infect Dis 26:338-44.
8. Shamsizadeh Z, Nikaeen M, Nasr Esfahani B, Mirhoseini SH, Hatamzadeh M, Hassanzadeh A. 2017. Detection of antibiotic resistant Acinetobacter baumannii in various hospital environments: potential sources for transmission of Acinetobacter infections. Environ Health Prev Med 22:44.
9. Catalano M, Quelle LS, Jeric PE, Di Martino A, Maimone SM. 1999. Survival of Acinetobacter baumannii on bed rails during an outbreak and during sporadic cases. J Hosp Infect 42:27-35.
10. Thom KA, Johnson JK, Lee MS, Harris AD. 2011. Environmental contamination because of multidrug-resistant Acinetobacter baumannii surrounding colonized or infected patients. Am J Infect Control 39:711-5.
11. Bayuga S, Zeana C, Sahni J, Della-Latta P, el-Sadr W, Larson E. 2002. Prevalence and antimicrobial patterns of Acinetobacter baumannii on hands and nares of hospital personnel and patients: the iceberg phenomenon again. Heart Lung 31:382-90.
12. Huang YC, Su LH, Wu TL, Leu HS, Hsieh WS, Chang TM, Lin TY. 2002. Outbreak of Acinetobacter baumannii bacteremia in a neonatal intensive care unit: clinical implications and genotyping analysis. Pediatr Infect Dis J 21:1105-9.
13. Morgan DJ, Liang SY, Smith CL, Johnson JK, Harris AD, Furuno JP, Thom KA, Snyder GM, Day HR, Perencevich EN. 2010. Frequent multidrug-resistant Acinetobacter baumannii contamination of gloves, gowns, and hands of healthcare workers. Infect Control Hosp Epidemiol 31:716-21.

14. Palmer LD, Minor KE, Mettlach JA, Rivera ES, Boyd KL, Caprioli RM, Spraggins JM, Dalebroux ZD, Skaar EP. 2020. Modulating Isoprenoid Biosynthesis Increases Lipooligosaccharides and Restores Acinetobacter baumannii Resistance to Host and Antibiotic Stress. Cell Rep 32:108129.
15. Harding CM, Hennon SW, Feldman MF. 2018. Uncovering the mechanisms of Acinetobacter baumannii virulence. Nat Rev Microbiol 16:91-102.
16. Espinal P, Marti S, Vila J. 2012. Effect of biofilm formation on the survival of Acinetobacter baumannii on dry surfaces. J Hosp Infect 80:56-60.
17. Montanaro L, Poggi A, Visai L, Ravaioli S, Campoccia D, Speziale P, Arciola CR. 2011. Extracellular DNA in biofilms. Int J Artif Organs 34:824-31.
18. Fong JNC, Yildiz FH. 2015. Biofilm Matrix Proteins. Microbiol Spectr 3.
19. Limoli DH, Jones CJ, Wozniak DJ. 2015. Bacterial Extracellular Polysaccharides in Biofilm Formation and Function. Microbiol Spectr 3.
20. Hall CW, Mah TF. 2017. Molecular mechanisms of biofilm-based antibiotic resistance and tolerance in pathogenic bacteria. FEMS Microbiol Rev 41:276-301.
21. Stewart PS. 2002. Mechanisms of antibiotic resistance in bacterial biofilms. Int J Med Microbiol 292:107-13.
22. Colquhoun JM, Rather PN. 2020. Insights Into Mechanisms of Biofilm Formation in Acinetobacter baumannii and Implications for Uropathogenesis. Front Cell Infect Microbiol 10:253.
23. Eze EC, Chenia HY, El Zowalaty ME. 2018. Acinetobacter baumannii biofilms: effects of physicochemical factors, virulence, antibiotic resistance determinants, gene regulation, and future antimicrobial treatments. Infect Drug Resist 11:2277-2299.
24. Tomaras AP, Dorsey CW, Edelmann RE, Actis LA. 2003. Attachment to and biofilm formation on abiotic surfaces by Acinetobacter baumannii: involvement of a novel chaperone-usher pili assembly system. Microbiology (Reading) 149:3473-3484.
25. Gaddy JA, Tomaras AP, Actis LA. 2009. The Acinetobacter baumannii 19606 OmpA protein plays a role in biofilm formation on abiotic surfaces and in the interaction of this pathogen with eukaryotic cells. Infect Immun 77:3150-60.
26. Pakharukova N, Tuittila M, Paavilainen S, Malmi H, Parilova O, Teneberg S, Knight SD, Zavialov AV. 2018. Structural basis for Acinetobacter baumannii biofilm formation. Proc Natl Acad Sci U S A 115:5558-5563.
27. Tomaras AP, Flagler MJ, Dorsey CW, Gaddy JA, Actis LA. 2008. Characterization of a two-component regulatory system from Acinetobacter baumannii that controls biofilm formation and cellular morphology. Microbiology (Reading) 154:3398-3409.
28. Geisinger E, Isberg RR. 2015. Antibiotic modulation of capsular exopolysaccharide and virulence in Acinetobacter baumannii. PLoS Pathog 11:e1004691.
29. Scott NE, Kinsella RL, Edwards AV, Larsen MR, Dutta S, Saba J, Foster LJ, Feldman MF. 2014. Diversity within the O-linked protein glycosylation systems of acinetobacter species. Mol Cell Proteomics 13:2354-70.
30. Ophir T, Gutnick DL. 1994. A role for exopolysaccharides in the protection of microorganisms from desiccation. Appl Environ Microbiol 60:740-5.

945 31. Eshwar AK, Guldimann C, Oevermann A, Tasara T. 2017. Cold-Shock Domain Family
946 Proteins (Csps) Are Involved in Regulation of Virulence, Cellular Aggregation, and
947 Flagella-Based Motility in Listeria monocytogenes. Front Cell Infect Microbiol 7:453.
948 32. White-Ziegler CA, Um S, Perez NM, Berns AL, Malhowski AJ, Young S. 2008. Low
949 temperature (23 degrees C) increases expression of biofilm-, cold-shock- and RpoS-
950 dependent genes in Escherichia coli K-12. Microbiology 154:148-66.
951 33. Keto-Timonen R, Hietala N, Palonen E, Hakakorpi A, Lindstrom M, Korkeala H. 2016. Cold
952 Shock Proteins: A Minireview with Special Emphasis on Csp-family of Enteropathogenic
953 Yersinia. Front Microbiol 7:1151.
954 34. Horn G, Hofweber R, Kremer W, Kalbitzer HR. 2007. Structure and function of bacterial
955 cold shock proteins. Cell Mol Life Sci 64:1457-70.
956 35. Phadtare S, Severinov K. 2010. RNA remodeling and gene regulation by cold shock
957 proteins. RNA Biol 7:788-95.
958 36. Salisbury V, Hedges RW, Datta N. 1972. Two modes of "curing" transmissible bacterial
959 plasmids. J Gen Microbiol 70:443-52.
960 37. Gallagher LA, Ramage E, Weiss EJ, Radey M, Hayden HS, Held KG, Huse HK, Zurawski DV,
961 Brittnacher MJ, Manoil C. 2015. Resources for Genetic and Genomic Analysis of
962 Emerging Pathogen Acinetobacter baumannii. J Bacteriol 197:2027-35.
963 38. Cassat JE, Lee CY, Smeltzer MS. 2007. Investigation of biofilm formation in clinical
964 isolates of Staphylococcus aureus. Methods Mol Biol 391:127-44.
965 39. Nadkarni MA, Martin FE, Jacques NA, Hunter N. 2002. Determination of bacterial load
966 by real-time PCR using a broad-range (universal) probe and primers set. Microbiology
967 148:257-266.
968 40. Fiester SE, Arivett BA, Schmidt RE, Beckett AC, Ticak T, Carrier MV, Ghosh R, Ohneck EJ,
969 Metz ML, Sellin Jeffries MK, Actis LA. 2016. Iron-Regulated Phospholipase C Activity
970 Contributes to the Cytolytic Activity and Virulence of Acinetobacter baumannii. PLoS
971 One 11:e0167068.
972 41. Abdi SN, Ghotaslou R, Asgharzadeh M, Mehramouz B, Hasani A, Baghi HB, Tanomand A,
973 Narenji H, Yousefi B, Gholizadeh P, Yousefi M, Bastami M, Ganbarov K, Samadi Kafil H.
974 2020. AdeB efflux pump gene knockdown by mRNA mediated peptide nucleic acid in
975 multidrug resistance Acinetobacter baumannii. Microb Pathog 139:103825.
976 42. Moon KH, Weber BS, Feldman MF. 2017. Subinhibitory Concentrations of Trimethoprim
977 and Sulfamethoxazole Prevent Biofilm Formation by Acinetobacter baumannii through
978 Inhibition of Csu Pilus Expression. Antimicrob Agents Chemother 61.
979 43. Amin IM, Richmond GE, Sen P, Koh TH, Piddock LJ, Chua KL. 2013. A method for
980 generating marker-less gene deletions in multidrug-resistant Acinetobacter baumannii.
981 BMC Microbiol 13:158.
982 44. Jacobs AC, Thompson MG, Gebhardt M, Corey BW, Yildirim S, Shuman HA, Zurawski DV.
983 2014. Genetic Manipulation of Acinetobacter baumannii. Curr Protoc Microbiol 35:6G 2
984 1-11.
985 45. Carroll RK, Weiss A, Shaw LN. 2016. RNA-Sequencing of Staphylococcus aureus
986 Messenger RNA. Methods Mol Biol 1373:131-41.
987 46. Robinson MD, Oshlack A. 2010. A scaling normalization method for differential
988 expression analysis of RNA-seq data. Genome Biol 11:R25.

47. Kanehisa M, Sato Y, Kawashima M, Furumichi M, Tanabe M. 2016. KEGG as a reference resource for gene and protein annotation. Nucleic Acids Res 44:D457-62.
48. Krzywinski M, Schein J, Birol I, Connors J, Gascoyne R, Horsman D, Jones SJ, Marra MA. 2009. Circos: an information aesthetic for comparative genomics. Genome Res 19:1639-45.
49. Schmittgen TD, Livak KJ. 2008. Analyzing real-time PCR data by the comparative C(T) method. Nat Protoc 3:1101-8.
50. Brzozowski RS, Tomlinson BR, Sacco MD, Chen JJ, Ali AN, Chen Y, Shaw LN, Eswara PJ. 2020. Interdependent YpsA- and YfhS-Mediated Cell Division and Cell Size Phenotypes in Bacillus subtilis. mSphere 5.
51. Tang L, Schramm A, Neu TR, Revsbech NP, Meyer RL. 2013. Extracellular DNA in adhesion and biofilm formation of four environmental isolates: a quantitative study. FEMS Microbiol Ecol 86:394-403.
52. Sager M, Benten WP, Engelhardt E, Gougoula C, Benga L. 2015. Characterization of Biofilm Formation in [Pasteurella] pneumotropica and [Actinobacillus] muris Isolates of Mouse Origin. PLoS One 10:e0138778.
53. Fleeman R, LaVoi TM, Santos RG, Morales A, Nefzi A, Welmaker GS, Medina-Franco JL, Giulianotti MA, Houghten RA, Shaw LN. 2015. Combinatorial Libraries As a Tool for the Discovery of Novel, Broad-Spectrum Antibacterial Agents Targeting the ESKAPE Pathogens. J Med Chem 58:3340-55.
54. de Castro E, Sigrist CJ, Gattiker A, Bulliard V, Langendijk-Genevaux PS, Gasteiger E, Bairoch A, Hulo N. 2006. ScanProsite: detection of PROSITE signature matches and ProRule-associated functional and structural residues in proteins. Nucleic Acids Res 34:W362-5.
55. Waterhouse A, Bertoni M, Bienert S, Studer G, Tauriello G, Gumienny R, Heer FT, de Beer TAP, Rempfer C, Bordoli L, Lepore R, Schwede T. 2018. SWISS-MODEL: homology modelling of protein structures and complexes. Nucleic Acids Res 46:W296-W303.
56. Schindelin H, Jiang W, Inouye M, Heinemann U. 1994. Crystal structure of CspA, the major cold shock protein of Escherichia coli. Proc Natl Acad Sci U S A 91:5119-23.
57. Ching C, Gozzi K, Heinemann B, Chai Y, Godoy VG. 2017. RNA-Mediated cis Regulation in Acinetobacter baumannii Modulates Stress-Induced Phenotypic Variation. J Bacteriol 199.
58. Wada T, Becskei A. 2017. Impact of Methods on the Measurement of mRNA Turnover. Int J Mol Sci 18.
59. Lorenz R, Bernhart SH, Honer Zu Siederdissen C, Tafer H, Flamm C, Stadler PF, Hofacker IL. 2011. ViennaRNA Package 2.0. Algorithms Mol Biol 6:26.
60. Kerpedjiev P, Hammer S, Hofacker IL. 2015. Forna (force-directed RNA): Simple and effective online RNA secondary structure diagrams. Bioinformatics 31:3377-9.
61. Kolar SL, Nagarajan V, Oszmiana A, Rivera FE, Miller HK, Davenport JE, Riordan JT, Potempa J, Barber DS, Koziel J, Elasri MO, Shaw LN. 2011. NsaRS is a cell-envelope-stress-sensing two-component system of Staphylococcus aureus. Microbiology (Reading) 157:2206-2219.
62. Sun D, Crowell SA, Harding CM, De Silva PM, Harrison A, Fernando DM, Mason KM, Santana E, Loewen PC, Kumar A, Liu Y. 2016. KatG and KatE confer Acinetobacter

resistance to hydrogen peroxide but sensitize bacteria to killing by phagocytic respiratory burst. Life Sci 148:31-40.

63. Palmer LD, Green ER, Sheldon JR, Skaar EP. 2019. Assessing Acinetobacter baumannii Virulence and Persistence in a Murine Model of Lung Infection. Methods Mol Biol 1946:289-305.

64. Choby JE, Monteith AJ, Himmel LE, Margaritis P, Shirey-Rice JK, Pruijssers A, Jerome RN, Pulley J, Skaar EP. 2019. A Phenome-Wide Association Study Uncovers a Pathological Role of Coagulation Factor X during Acinetobacter baumannii Infection. Infect Immun 87.

65. Casella LG, Weiss A, Perez-Rueda E, Antonio Ibarra J, Shaw LN. 2017. Towards the complete proteinaceous regulome of Acinetobacter baumannii. Microb Genom 3:mgen000107.

66. Wang N, Ozer EA, Mandel MJ, Hauser AR. 2014. Genome-wide identification of Acinetobacter baumannii genes necessary for persistence in the lung. mBio 5:e01163-14.

67. Gebhardt MJ, Gallagher LA, Jacobson RK, Usacheva EA, Peterson LR, Zurawski DV, Shuman HA. 2015. Joint Transcriptional Control of Virulence and Resistance to Antibiotic and Environmental Stress in Acinetobacter baumannii. mBio 6:e01660-15.

68. Kanehisa M, Goto S. 2000. KEGG: kyoto encyclopedia of genes and genomes. Nucleic Acids Res 28:27-30.

69. Kroger C, MacKenzie KD, Alshabib EY, Kirzinger MWB, Suchan DM, Chao TC, Akulova V, Miranda-CasoLuengo AA, Monzon VA, Conway T, Sivasankaran SK, Hinton JCD, Hokamp K, Cameron ADS. 2018. The primary transcriptome, small RNAs and regulation of antimicrobial resistance in Acinetobacter baumannii ATCC 17978. Nucleic Acids Res 46:9684-9698.

70. Gutierrez D, Hidalgo-Cantabrana C, Rodriguez A, Garcia P, Ruas-Madiedo P. 2016. Monitoring in Real Time the Formation and Removal of Biofilms from Clinical Related Pathogens Using an Impedance-Based Technology. PLoS One 11:e0163966.

71. Biosciences A. 2013. Dynamic Monitoring of Cell Adhesion and Spreading. ACEA Biosciences, Inc.

72. Loh B, Chen J, Manohar P, Yu Y, Hua X, Leptihn S. 2020. A Biological Inventory of Prophages in A. baumannii Genomes Reveal Distinct Distributions in Classes, Length, and Genomic Positions. Front Microbiol 11:579802.

73. Rumbo-Feal S, Gomez MJ, Gayoso C, Alvarez-Fraga L, Cabral MP, Aransay AM, Rodriguez-Ezpeleta N, Fullaondo A, Valle J, Tomas M, Bou G, Poza M. 2013. Whole transcriptome analysis of Acinetobacter baumannii assessed by RNA-sequencing reveals different mRNA expression profiles in biofilm compared to planktonic cells. PLoS One 8:e72968.

74. Coyne S, Rosenfeld N, Lambert T, Courvalin P, Perichon B. 2010. Overexpression of resistance-nodulation-cell division pump AdeFGH confers multidrug resistance in Acinetobacter baumannii. Antimicrob Agents Chemother 54:4389-93.

75. He X, Lu F, Yuan F, Jiang D, Zhao P, Zhu J, Cheng H, Cao J, Lu G. 2015. Biofilm Formation Caused by Clinical Acinetobacter baumannii Isolates Is Associated with Overexpression of the AdeFGH Efflux Pump. Antimicrob Agents Chemother 59:4817-25.

76. Damier-Piolle L, Magnet S, Bremont S, Lambert T, Courvalin P. 2008. AdeIJK, a resistance-nodulation-cell division pump effluxing multiple antibiotics in Acinetobacter baumannii. Antimicrob Agents Chemother 52:557-62.
77. Srinivasan VB, Rajamohan G, Gebreyes WA. 2009. Role of AbeS, a novel efflux pump of the SMR family of transporters, in resistance to antimicrobial agents in Acinetobacter baumannii. Antimicrob Agents Chemother 53:5312-6.
78. Yoon EJ, Chabane YN, Goussard S, Snesrud E, Courvalin P, De E, Grillot-Courvalin C. 2015. Contribution of resistance-nodulation-cell division efflux systems to antibiotic resistance and biofilm formation in Acinetobacter baumannii. mBio 6.
79. Geisinger E, Mortman NJ, Vargas-Cuebas G, Tai AK, Isberg RR. 2018. A global regulatory system links virulence and antibiotic resistance to envelope homeostasis in Acinetobacter baumannii. PLoS Pathog 14:e1007030.
80. Leus IV, Adamiak J, Trinh AN, Smith RD, Smith L, Richardson S, Ernst RK, Zgurskaya HI. 2020. Inactivation of AdeABC and AdeIJK efflux pumps elicits specific nonoverlapping transcriptional and phenotypic responses in Acinetobacter baumannii. Mol Microbiol doi:10.1111/mmi.14594.
81. Magnet S, Courvalin P, Lambert T. 2001. Resistance-nodulation-cell division-type efflux pump involved in aminoglycoside resistance in Acinetobacter baumannii strain BM4454. Antimicrob Agents Chemother 45:3375-80.
82. Leus IV, Adamiak J, Trinh AN, Smith RD, Smith L, Richardson S, Ernst RK, Zgurskaya HI. 2020. Inactivation of AdeABC and AdeIJK efflux pumps elicits specific nonoverlapping transcriptional and phenotypic responses in Acinetobacter baumannii. Mol Microbiol 114:1049-1065.
83. Murzin AG. 1993. OB(oligonucleotide/oligosaccharide binding)-fold: common structural and functional solution for non-homologous sequences. EMBO J 12:861-7.
84. Theobald DL, Mitton-Fry RM, Wuttke DS. 2003. Nucleic acid recognition by OB-fold proteins. Annu Rev Biophys Biomol Struct 32:115-33.
85. Bernstein JA, Lin PH, Cohen SN, Lin-Chao S. 2004. Global analysis of Escherichia coli RNA degradosome function using DNA microarrays. Proc Natl Acad Sci U S A 101:2758-63.
86. Selinger DW, Saxena RM, Cheung KJ, Church GM, Rosenow C. 2003. Global RNA half-life analysis in Escherichia coli reveals positional patterns of transcript degradation. Genome Res 13:216-23.
87. Roberts C, Anderson KL, Murphy E, Projan SJ, Mounts W, Hurlburt B, Smeltzer M, Overbeek R, Disz T, Dunman PM. 2006. Characterizing the effect of the Staphylococcus aureus virulence factor regulator, SarA, on log-phase mRNA half-lives. J Bacteriol 188:2593-603.
88. Hambraeus G, von Wachenfeldt C, Hederstedt L. 2003. Genome-wide survey of mRNA half-lives in Bacillus subtilis identifies extremely stable mRNAs. Mol Genet Genomics 269:706-14.
89. Esquerre T, Moisan A, Chiapello H, Arike L, Vilu R, Gaspin C, Cocaign-Bousquet M, Girbal L. 2015. Genome-wide investigation of mRNA lifetime determinants in Escherichia coli cells cultured at different growth rates. BMC Genomics 16:275.

90. Qing G, Xia B, Inouye M. 2003. Enhancement of translation initiation by A/T-rich sequences downstream of the initiation codon in Escherichia coli. J Mol Microbiol Biotechnol 6:133-44.
91. Monem S, Furmanek-Blaszk B, Lupkowska A, Kuczynska-Wisnik D, Stojowska-Swedrzynska K, Laskowska E. 2020. Mechanisms Protecting Acinetobacter baumannii against Multiple Stresses Triggered by the Host Immune Response, Antibiotics and Outside-Host Environment. Int J Mol Sci 21.
92. Ozkul C, Hazirolan G. 2020. Oxacillinase Gene Distribution, Antibiotic Resistance, and Their Correlation with Biofilm Formation in Acinetobacter baumannii Bloodstream Isolates. Microb Drug Resist doi:10.1089/mdr.2020.0130.
93. Marks LR, Davidson BA, Knight PR, Hakansson AP. 2013. Interkingdom signaling induces Streptococcus pneumoniae biofilm dispersion and transition from asymptomatic colonization to disease. mBio 4.
94. Qiu H, Kuolee R, Harris G, Chen W. 2009. Role of NADPH phagocyte oxidase in host defense against acute respiratory Acinetobacter baumannii infection in mice. Infect Immun 77:1015-21.
95. Juttukonda LJ, Green ER, Lonergan ZR, Heffern MC, Chang CJ, Skaar EP. 2019. Acinetobacter baumannii OxyR Regulates the Transcriptional Response to Hydrogen Peroxide. Infect Immun 87.
96. Marqués MaLG. 2018. Hypoxia effect on genetic regulation and virulence in *Acinetobacter baumannii* and *Pseudomonas aeruginosa,* in vitro and in vivo, and on innate immune response in infections caused by both pathogens. Doctoral. Universidad de Sevilla, Seville.
97. Cendra MDM, Blanco-Cabra N, Pedraz L, Torrents E. 2019. Optimal environmental and culture conditions allow the in vitro coexistence of Pseudomonas aeruginosa and Staphylococcus aureus in stable biofilms. Sci Rep 9:16284.
98. Rani SA, Pitts B, Beyenal H, Veluchamy RA, Lewandowski Z, Davison WM, Buckingham-Meyer K, Stewart PS. 2007. Spatial patterns of DNA replication, protein synthesis, and oxygen concentration within bacterial biofilms reveal diverse physiological states. J Bacteriol 189:4223-33.
99. Wassarman KM, Storz G. 2000. 6S RNA regulates E. coli RNA polymerase activity. Cell 101:613-23.
100. Trotochaud AE, Wassarman KM. 2004. 6S RNA function enhances long-term cell survival. J Bacteriol 186:4978-85.
101. Schmid B, Klumpp J, Raimann E, Loessner MJ, Stephan R, Tasara T. 2009. Role of cold shock proteins in growth of Listeria monocytogenes under cold and osmotic stress conditions. Appl Environ Microbiol 75:1621-7.
102. Derman Y, Soderholm H, Lindstrom M, Korkeala H. 2015. Role of csp genes in NaCl, pH, and ethanol stress response and motility in Clostridium botulinum ATCC 3502. Food Microbiol 46:463-470.
103. Duval BD, Mathew A, Satola SW, Shafer WM. 2010. Altered growth, pigmentation, and antimicrobial susceptibility properties of Staphylococcus aureus due to loss of the major cold shock gene cspB. Antimicrob Agents Chemother 54:2283-90.

104. Amin M, Navidifar T, Shooshtari FS, Rashno M, Savari M, Jahangirmehr F, Arshadi M. 2019. Association Between Biofilm Formation, Structure, and the Expression Levels of Genes Related to biofilm formation and Biofilm-Specific Resistance of Acinetobacter baumannii Strains Isolated from Burn Infection in Ahvaz, Iran. Infect Drug Resist 12:3867-3881.

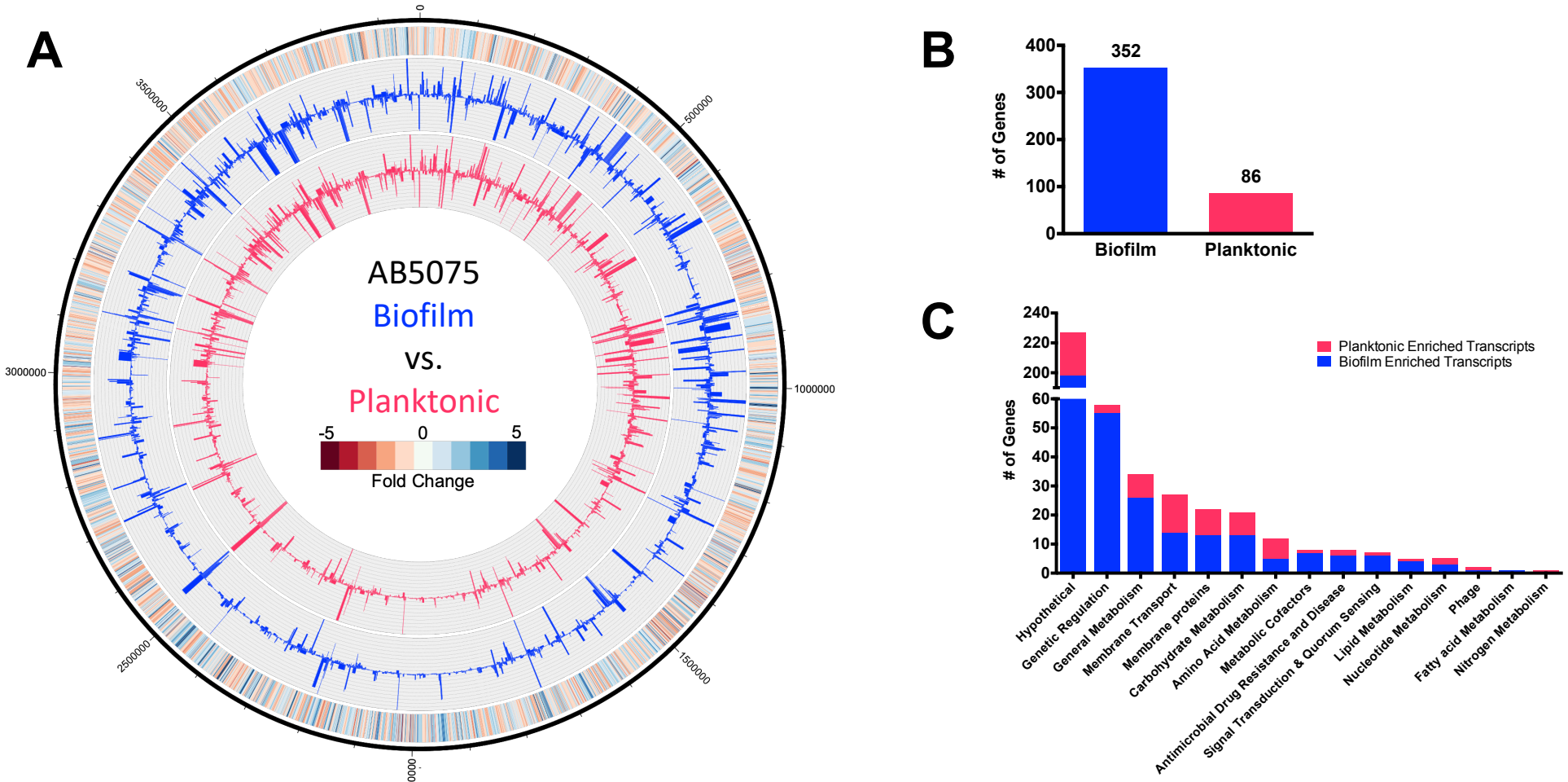

Figure 1. *A. baumannii* biofilms exhibit differential expression patterns compared to planktonic cell populations. The genomic map (**A**) depicts changes in planktonic (inner circle, pink) and biofilm (outer circle, blue) transcriptomes, reported as TPM expression values. The outermost circle is a heat map demonstrating fold change in expression, where red or blue indicates higher expression in the biofilm or planktonic cells, respectively. The number of genes that were preferentially expressed ≥2-fold in biofilm (blue) or planktonic (pink) cell populations are tallied (**B**) and further sorted by function based on KEGG ontology (**C**).

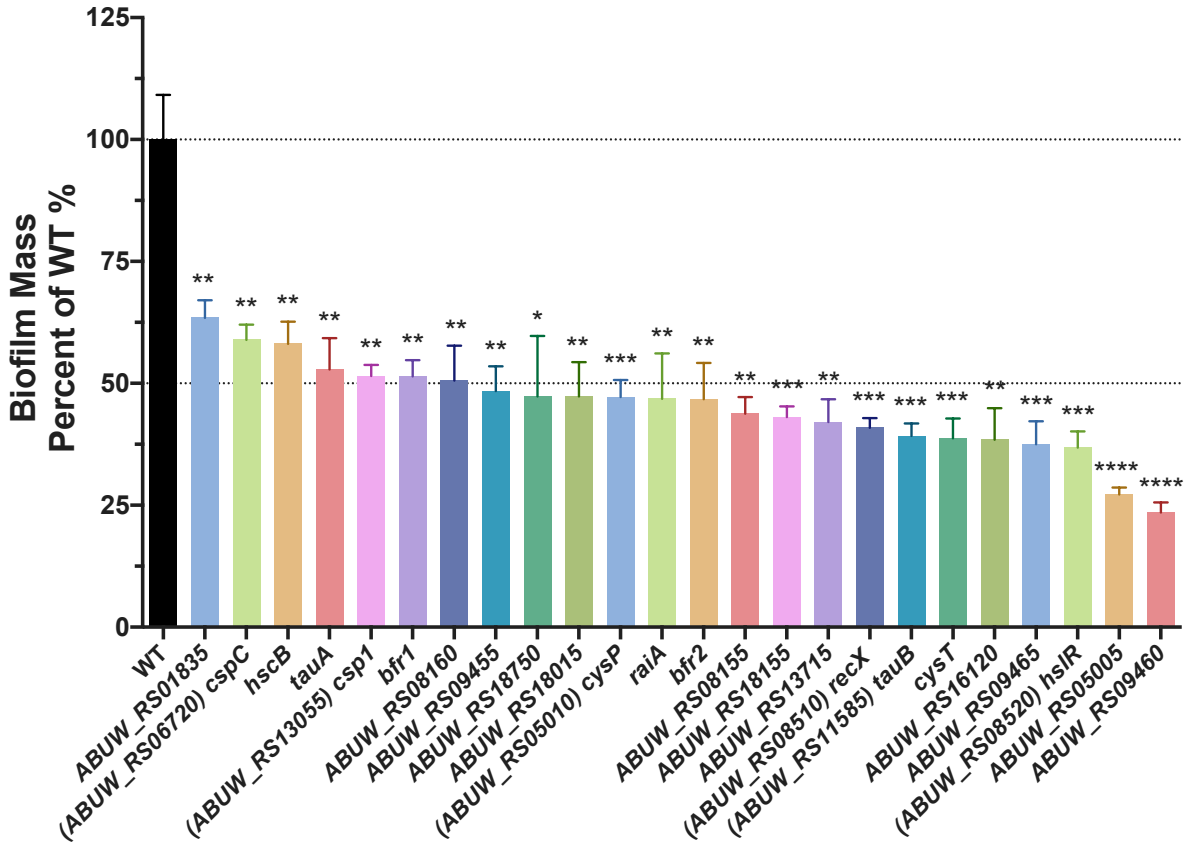

Figure 2. Physiological impact of gene disruption for those preferentially expressed in biofilms. Crystal violet biofilm assays were performed with transposon mutants of select genes preferentially expressed within biofilms. Alterations in biofilm mass are reported as a percentage of wildtype. Assays were performed in biological triplicate with 3 technical replicates each. Error bars represent ±SEM, Student's *t* test was used to determine statistical significance. *, P≤0.05; **, P≤0.01; ***, P≤0.001; **** P≤0.0001.

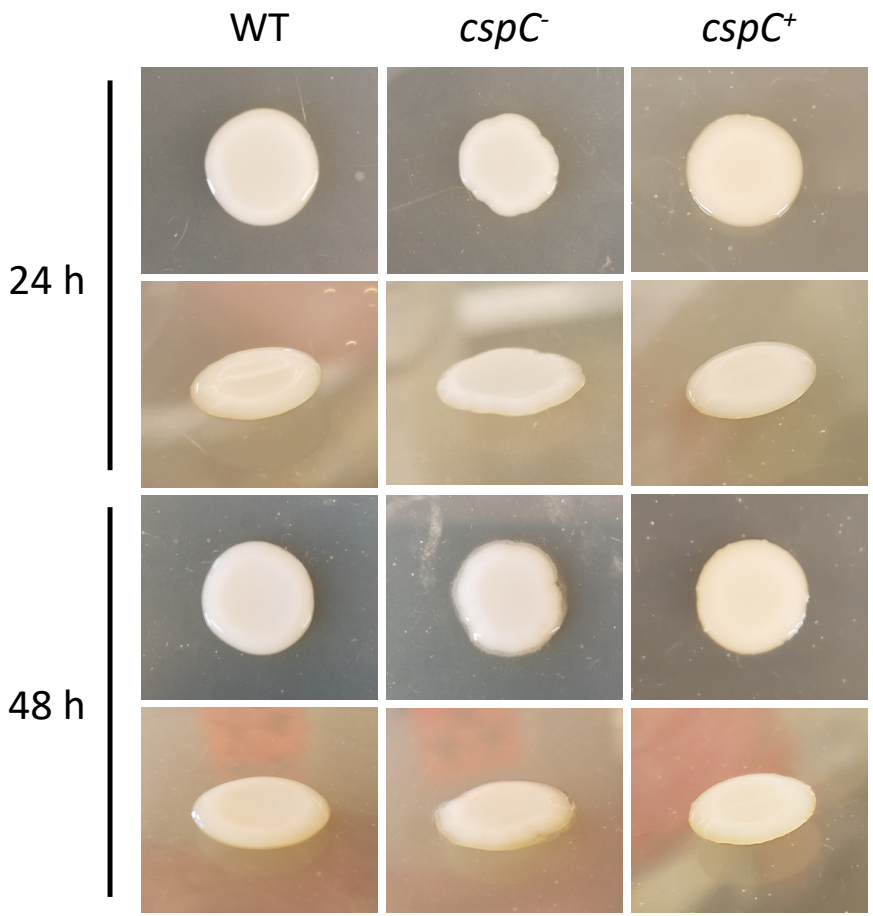

Figure 3. *cspC* mutants display an altered colony morphology. Wildtype (WT), *cspC*$^{-}$, and *cspC*$^{+}$ strains were grown on LB agar supplemented with hygromycin at 37°C for 24 h (top) and subsequently left to grow for an additional 24h at room temperature (bottom). Images are representative of 3 experimental repeats.

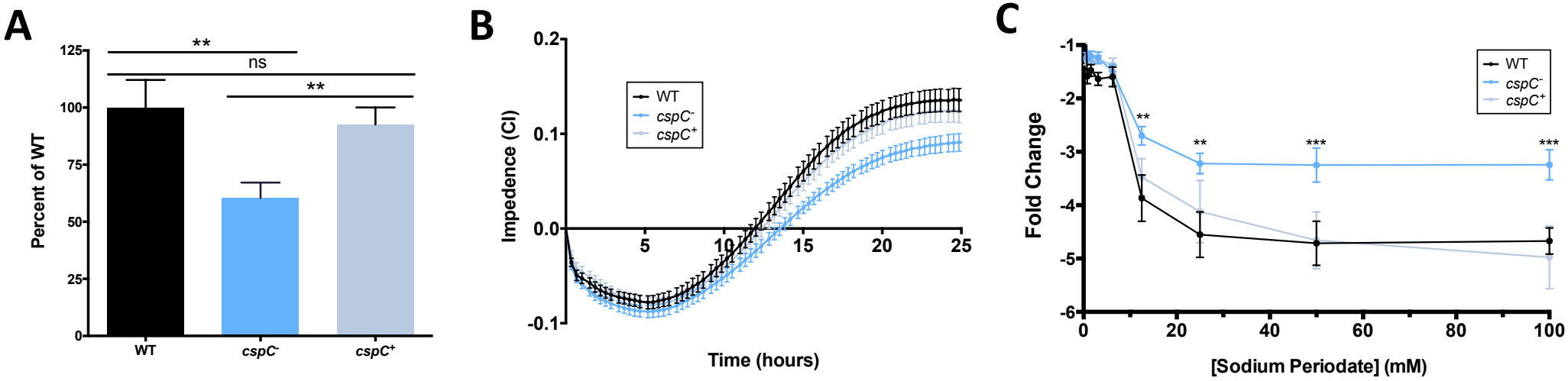

Figure 4. Disruption of *cspC* results in impaired biofilm formation and enhanced resistance to sodium periodate disruption. Comparison of biofilm formation using crystal violet staining following 24 hours growth (**A**), and continuously using an RTCA-xCELLigence (**B**) over a 25 h period. Assays were performed in biological triplicate with 3 technical replicates each. Error bars represent ±SEM; Student's *t*-test was used to determine statistical significance compared to wildtype. **, P≤0.01, ns = not significant. For biofilm inhibition assay (**C**), biofilms were seeded with increasing concentrations of sodium periodate and incubated for 24h, with the resulting biofilms measured using a crystal violet assay. Data points are from 10 biological replicates and 3 technical replicates. Fold change is reported relative to no treatment controls for each strain. Error bars represent ±SEM. A two-way ANOVA was used to determine statistical significance from the wild type. **, P≤0.01; ***, P≤0.001.

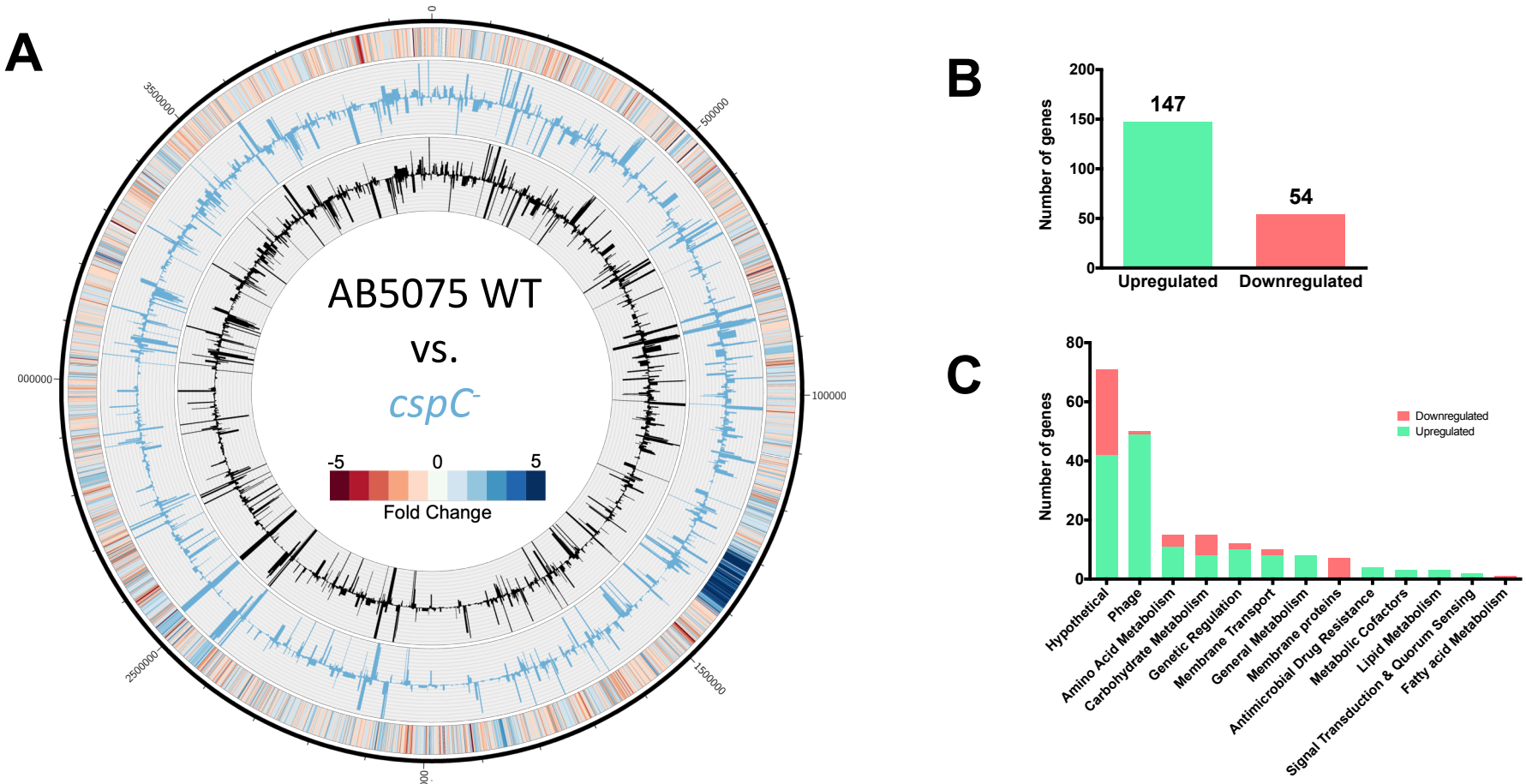

Figure 5. *A. baumannii* *cspC* disruption leads to global transcriptional changes. The genomic map (**A**) depicts transcription profiles of the wildtype and *cspC* mutant reported as TPM expression values. Inner histograms display RNA-seq expression values of the wildtype (black) and *cspC* mutant (blue) reported as TPM. The outermost circle is a heat map illustrating fold change in expression upon *cspC* disruption relative to wildtype, where blue or red indicates the fold-increase or -decrease of expression, respectively. The number of genes upregulated ≥2-fold (green) or downregulated (red) are tallied (**B**), and parsed by function based on KEGG ontology (**C**).

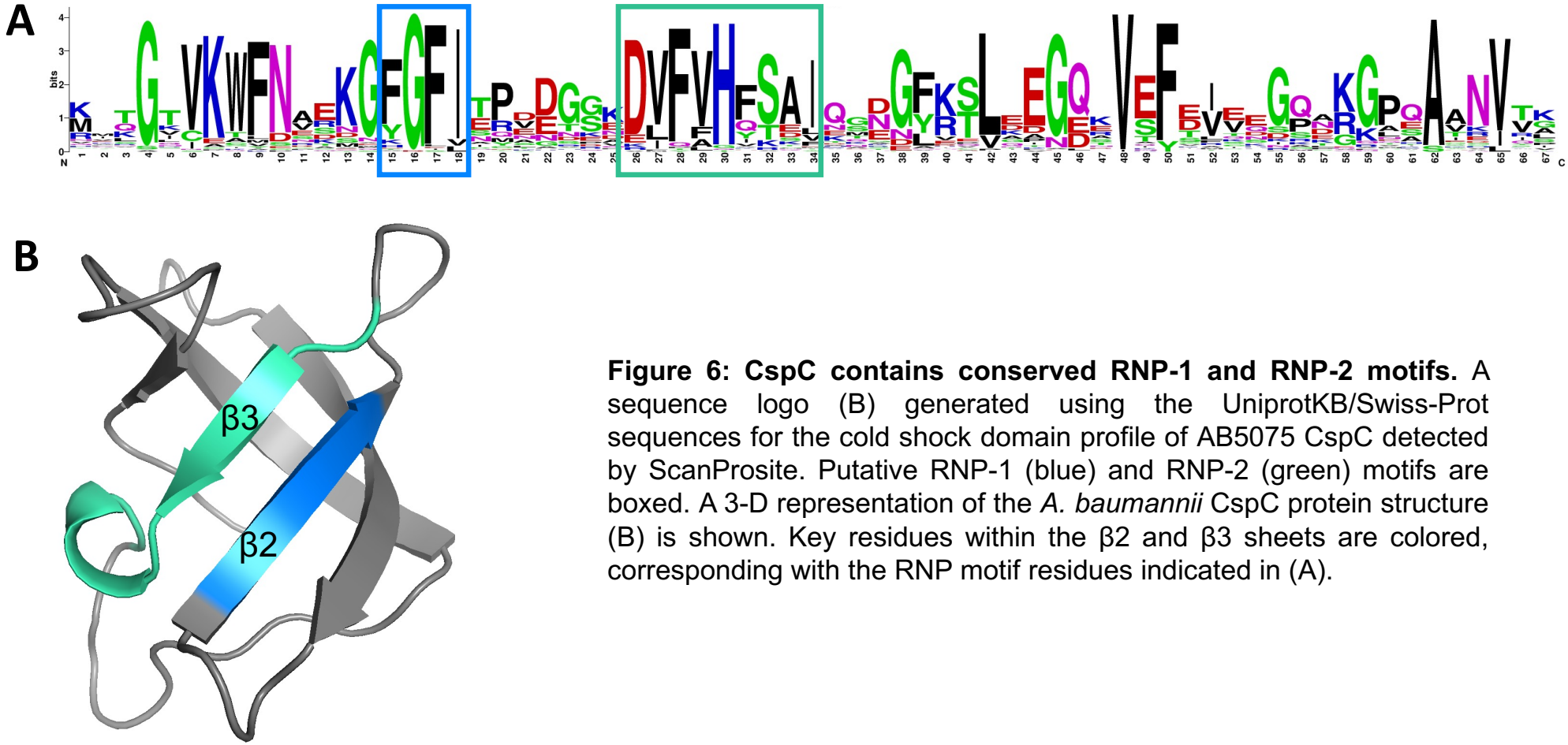

Figure 6: CspC contains conserved RNP-1 and RNP-2 motifs. A sequence logo (B) generated using the UniprotKB/Swiss-Prot sequences for the cold shock domain profile of AB5075 CspC detected by ScanProsite. Putative RNP-1 (blue) and RNP-2 (green) motifs are boxed. A 3-D representation of the *A. baumannii* CspC protein structure (B) is shown. Key residues within the β2 and β3 sheets are colored, corresponding with the RNP motif residues indicated in (A).

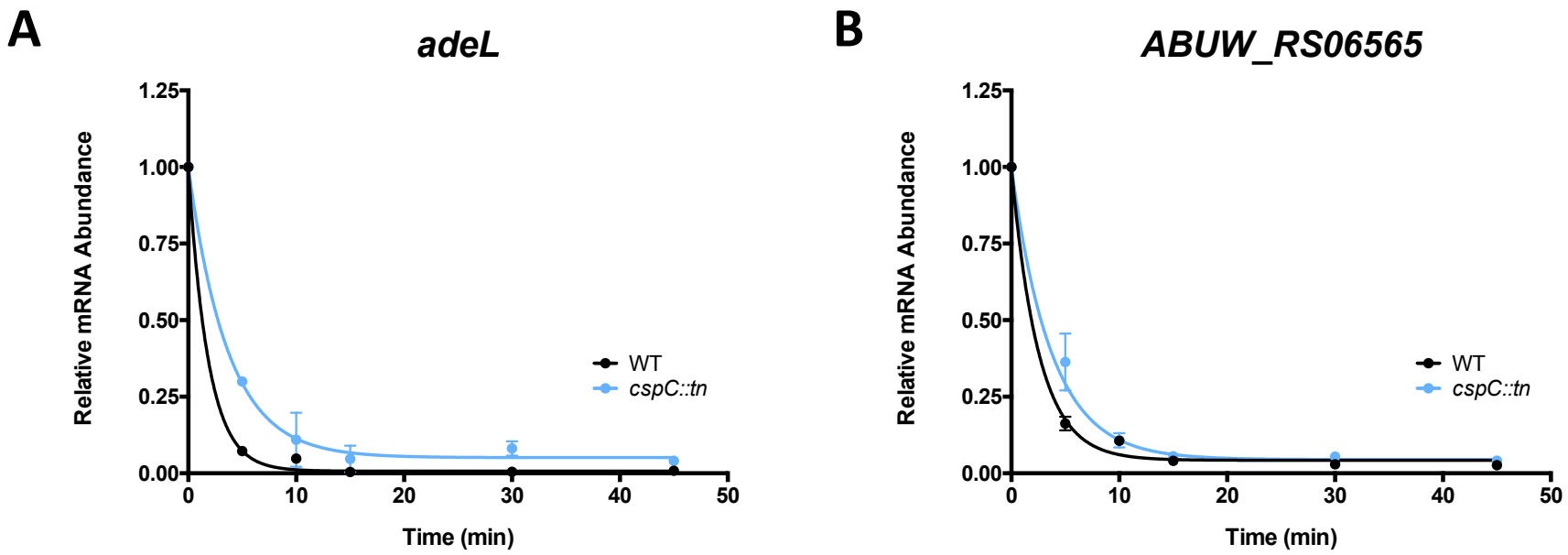

Figure 7. CspC mutation results in extended mRNA half life for transcriptional regulators, *adeL* and *ABUW_RS06565*. Exponentially growing *A. baumannii* wildtype and cspC mutant strains were treated with 250 µg/mL rifampin to arrest transcription and changes in transcript abundance was measured by RT-qPCR for *adeL* (A) and *ABUW_RS06565* (B). Values represent mean fold change in transcript abundance relative to transcript abundance immediately prior to rifampin treatment (t=0) ± standard deviation. Lines represent the exponential, one phase decay curve, represented as $R(t) = R_0 e^{-kt}$, which were used to calculate mRNA half lives.

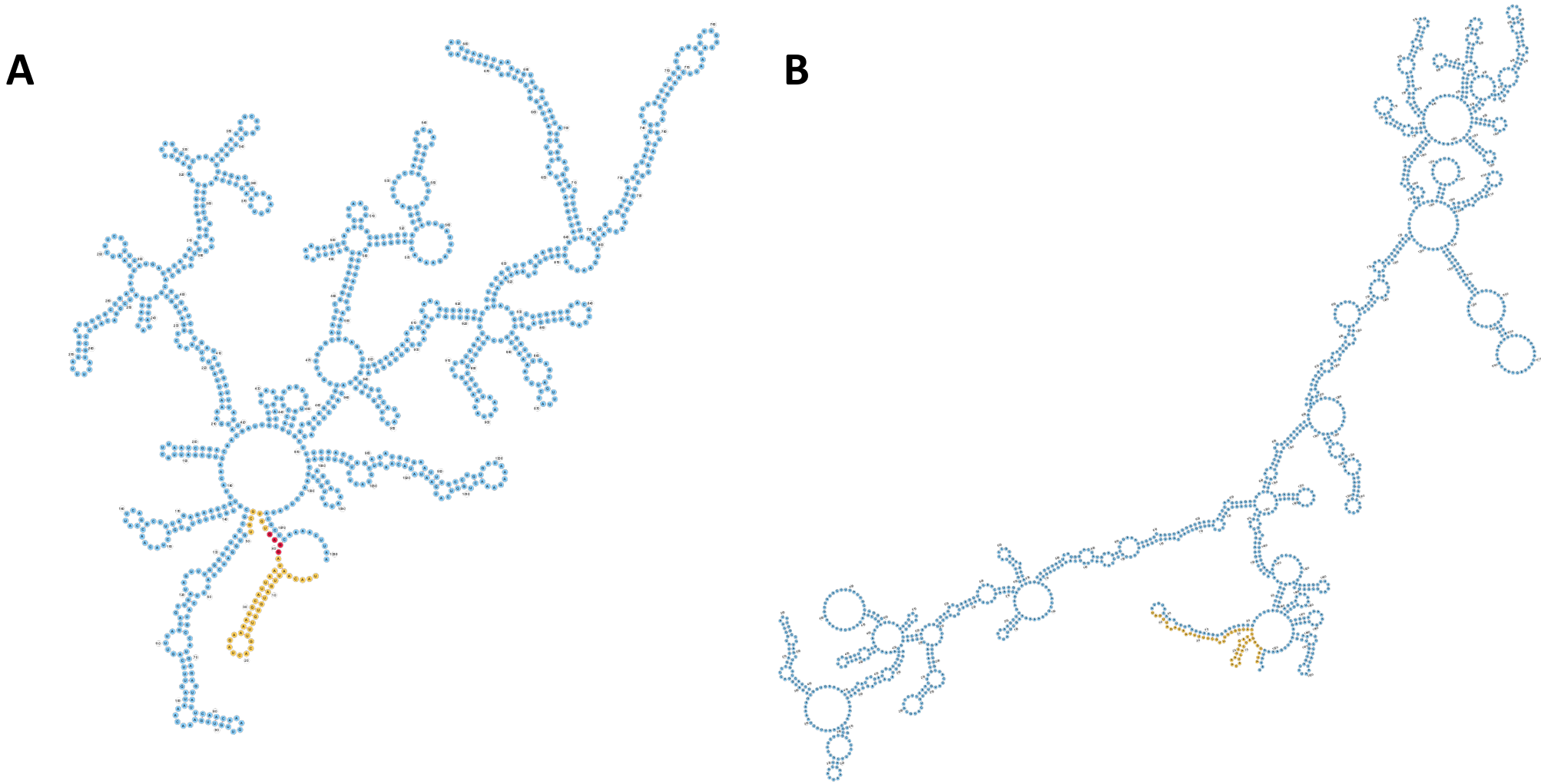

Figure 8. 5'UTR of *adeL* mRNA contains a stable structure in close proximity to the putative ribosomal binding site. The secondary structure for *adeL* (A) and *ABUW_RS06565* (B) mRNA predicted using RNAfold is shown. Nucleotide colors correspond to the 5'UTR (yellow), putative ribosomal binding site (red), and protein coding sequence (blue). For *ABUW_RS06565,* a ribosomal binding site was not apparent.

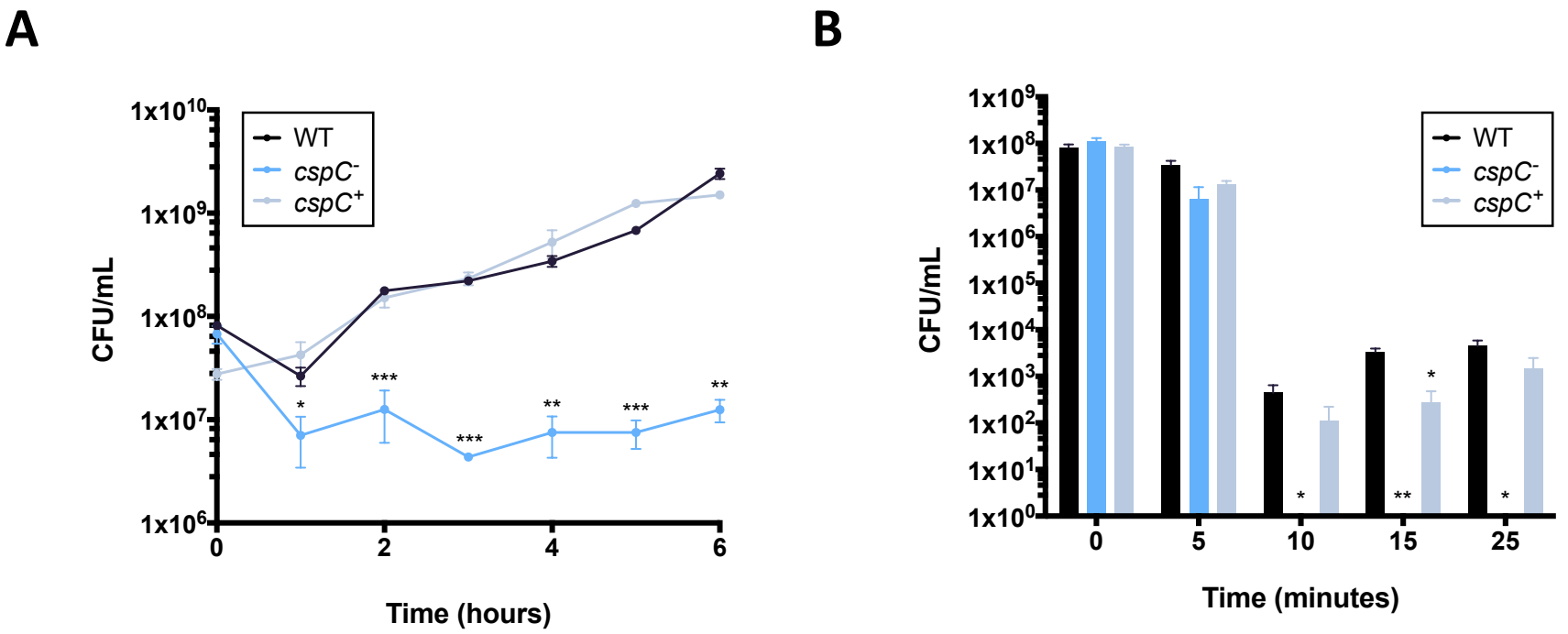

Figure 9. The *cspC* mutant has abrogated survival in human blood and during oxidative stress. Cell viability of the *cspC* mutant was assessed in whole human blood (**A**) and in the presence of 2mM hydrogen peroxide (**B**). Assays were performed in biological triplicate. Data is presented as the mean and error bars represent ±SEM. Student's *t* test was used to determine statistical difference to wildtype at each timepoint. *, P≤0.05; **, P≤0.01; ***, P≤0.001.

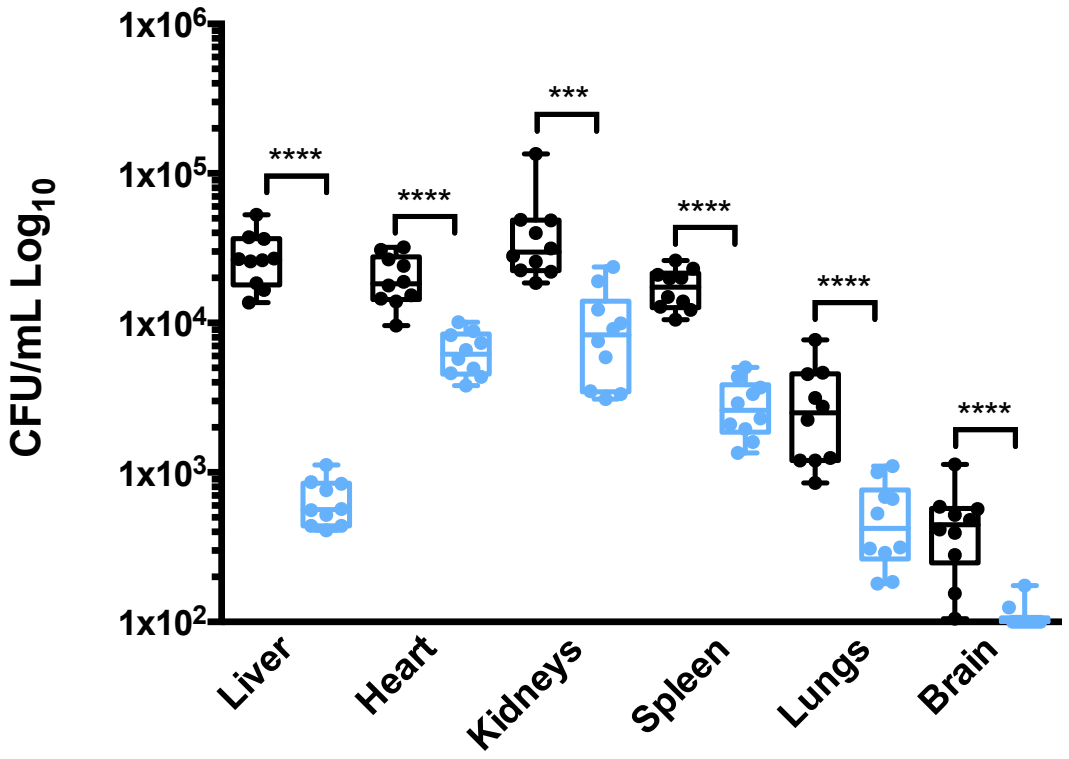

Figure 10. The *cspC* mutant is attenuated virulence for virulence in a murine model of sepsis. Cohorts of BL/6 mice (*n* = 10) were inoculated by retro orbital injection with 2.5x10^7 CFU of wildtype (black) and *cspC::tn* mutant strains (blue). At 6 h post infection, mice were euthanized, and organs were collected to determine bacterial load. The bounds of each box represents 25th-75th percentiles, whiskers represent 5th-95th percentiles, center line denotes the median, and individual data points are plotted as circles. Statistical significance was determined using a Mann-Whitney nonparametric test. ***, P<0.001; ****, P <0.0001.

Table 1. Bacterial strains and plasmids used in this study.

Strains	Description	Source
E. coli		
DH5α	Cloning strain	(36)
A. baumannii		
AB5075	Parent strain	(37)
cspC::tn	AB5075 with transposon insertion in ABUW_1377 (*cspC*)	(37)
WT	AB5075 containing pMQ557	This study
cspC^{-}	*cspC::tn* containing pMQ557	This study
cspC^{+}	*cspC::tn* containing pMQ557::*cspC*	This study
Plasmids		
pMQ557	Cloning vector for complementation	Gift, Dr. R. Shanks, University of Pittsburgh
pLSBT1	pMQ557::*cspC*	This study

Table 2. Prioritized genes exhibiting preferential expression within biofilms.

Gene	Expression (TPM)[†]	Fold Change[‡]
ssrS	62175.62	3.15
ffs	4153.04	3.38
leuA	1513.08	3.55
cspC (ABUW_RS06720)	1324.94	3.16
hslR (ABUW_RS08520)	1059.73	3.24
ABUW_RS08155	1037.86	3.58
ABUW_RS02640	737.36	3.18
ABUW_RS09455	717.76	3.53
cysD	565.84	3.95
ABUW_RS01835	554.93	3.92
bfr_2	532.31	3.36
ABUW_RS08160	511.43	4.02
cysP (ABUW_RS05010)	440.27	51.8
iscA	370.19	3.93
ABUW_RS20285	330.21	3.71
csp1 (ABUW_RS13055)	325.75	15.48
ABUW_RS09460	322.14	3.07
raiA	318.52	3.65
ABUW_RS05005	293.8	60.17
tauA	242.59	16
ABUW_RS18750	211.35	3.98
tauB (ABUW_RS11585)	207.38	15.64
ABUW_RS09465	184.01	3.96
ABUW_RS04445	175.35	7.93
hscB	167.95	3.53
ABUW_RS16120	165.53	3.66
ABUW_RS17360	163.51	3.24
ABUW_RS20445	160.93	17.11
ABUW_RS10540	153.08	12.13
ABUW_RS01965	152.46	3.17
recX (ABUW_RS08510)	145.88	4.62
tauC	138.39	11.13
ABUW_RS18155	136.84	5.31
ABUW_RS07450	133.65	9.93
ABUW_RS09695	131.04	3.56
ABUW_RS13715	128.98	3.94
ABUW_RS18015	122.17	4.61
cysT	121.76	30.66
tauD	118.66	7.69
bfr_1	115.41	3.43

[†]Expression is reported as TPM of biofilm sample measured by RNA-seq
[‡]Fold change is reported as expression of biofilm relative to planktonic sample

Table 3. Antibiotic susceptibility of AB5075 wildtype and *cspC* mutant strain (µg/mL).

Strain	CIP	CM	STR	GM	KAN	NEO	FOS	OX
AB5075 wildtype	45	84.38	1070	2000	2250	253.13	562.5	1130
AB5075 *cspC::tn*	80	150	3380	1500	1690	189.84	316.41	1130

Abbreviations: CIP, ciprofloxacin; CM, chloramphenicol; STR, streptomycin; GM, gentamicin; KAN, kanamycin; NEO, neomycin; FOS, fosfomycin; OX, oxacillin.

Table 4. Mean mRNA half-lives of CspC-regulated transcripts as determined by RNA decay assays.

Gene	Wildtype			*cspC::tn*		
	Half-life (min)*	**Decay constant (*k*)** †	**R^2**	**Half-life (min)***	**Decay constant (*k*)**	**R^2**
adeJ	5.326	0.1301±0.015	0.954	5.206	0.1331±0.020	0.928
adeG	4.773	0.1452±0.016	0.926	4.236	0.1636±0.024	0.884
adeL	1.280	0.5417±0.020	0.999	2.540	0.2728±0.022	0.969
ABUW_RS06565	1.753	0.396±0.025	0.990	2.565	0.270±0.016	0.993
recA	4.674	0.1483±0.002	0.999	4.890	0.1418±0.031	0.880

*The decay constant (k) mean was used to calculate half-life using $t_{1/2} = \ln(2)/k$, where $t_{1/2}$ represents mRNA half-life.

†Decay constant is reported as mean ± standard error.